Population Transcriptome and Phenotype Reveal that the *Rht-D1b* Contribute a Larger Seedling Roots to Modern Wheat Cultivars

Xiaoming Wang[1,3], Peng Zhao[1,3], Xiaolong Guo[1,3], Zihui, Liu[1], Xiuyun Ma[1], Yuqian Zhao[1], Xiangjun Lai[1], Liuying Huang[1], Wanying Wang[1], Dejun Han[1], Zhensheng Kang[2,*], Shengbao Xu[1,*]

[1]State Key Laboratory of Crop Stress Biology for Arid Areas, College of Agronomy, Northwest A&F University, Yangling, Shaanxi 712100, China.

[2]State Key Laboratory of Crop Stress Biology for Arid Areas, College of Plant Protection, Northwest A&F University, Yangling, Shaanxi 712100, China.

[3] These authors contributed equally to this article.

*** Correspondence:** Shengbao Xu (xushb@nwsuaf.edu.cn), Zhensheng Kang (kangzs@nwsuaf.edu.cn)

Running Title: *Rht-D1b* alters the modern wheat root

Short Summary: *Rht-D1b* is the major allele that contribute a larger root system and higher root-shoot ratio to modern wheat cultivars.

ABSTRACT

The crop root system is pivotal for water and nutrient uptake. Although the breeding selection significantly increased the yield of modern wheat cultivars, then how this selection reshapes the root system remains largely unknown. Here we performed a large-scale transcriptomic and phenotypical investigations on the seedling root of 406 wheat accessions, which demonstrated modern cultivars (MC) had significantly changed in the root transcriptome and root development. The MC had a significantly larger seedling root system than that in landraces (LA), and this was mainly due to the *Rht-D1b* allele introduction. Physiological and cytological investigations showed that the *Rht-D1b* suppressed gibberellin (GA) signaling, thus inhibiting the cell length in above-ground tissue but increasing the cell length in roots. This distinct regulation of GA signaling between above- and under-ground tissues contributed to MC having a significantly larger root-shoot ratio. Moreover, *Rht-D1b* also has a GA-independent role to enlarge root cell width that enhanced the root diameter, ultimately contribute to a larger root surface and volume to MC seedlings. These findings provide new insights to understand the successful application of GA-suppressing alleles in modern wheat breeding and its futural application to form a robust wheat root system.

Key words: wheat, roots system, *Rht-D1b*, population transcriptome

INTRODUCTION

Roots are the fundamental system used for water and nutrient uptake (Den Herder et al., 2010; van der Bom et al., 2020), and play the critical role in plant abiotic stresses adaptation (Calleja-Cabrera et al., 2020; de Vries et al., 2020; Hu et al., 2019; Khan et al., 2016; Lynch, 1995). The monocotyledonous wheat root is composed of seminal and adventitious roots. The seminal root system are the first to develop and they consist of the primary root and two pairs of seminal roots (Hendel et al., 2021; Hou et al., 2019). Seminal roots penetrate the soil earlier and deeper than adventitious roots and remain active throughout the plant life cycle, thereby play crucial roles in absorbing water from deep soil layers (Watt et al., 2008) and maintaining the survival during drought (Bacher et al., 2021; Golan et al., 2018).

Modern bread wheat (*Triticum aestivum* L.) is a hexaploidy comprising A, B, and D subgenomes (IWGSC, 2018; Zhou et al., 2020). During wheat evolution and domestication, the roots had experienced a suite of complex genetic, morphological and physiological function modifications (Abbo et al., 2014; Golan et al., 2018), including increased drought tolerance (Bacher et al., 2021; Golan et al., 2018). Over the past century, wheat grain yield has been remarkably improved with the breeding activities targeting high-yield (Godfray et al., 2010; Snowdon et al., 2020; van de Wouw et al., 2010). This breeding selection largely altered the wheat genome and differentiated modern cultivars (MC) from landraces (LA) (Hao et al., 2020; Hu et al., 2019; Zhou et al., 2020). Significantly, the Green Revolution of the 1960s, by introducing semi-dwarfing genes into rice and wheat, dramatically increased cereal grain yields with the higher levels input of inorganic nitrogen-based fertilizers (Pearce et al., 2011; Van De Velde et al., 2021). Then, how the roots of MC adapt to current cultivation practices remain largely unknown.

In hexaploid wheat, dwarfing has been achieved mainly through the introduction of the *Rht* (Reduced height) alleles *Rht-B1b* and *Rht-D1b* (also named *Rht1* and *Rht2*), which introduce premature stop codons in the N-terminal coding region of DELLA proteins, blocking the gibberellin (GA) signaling (Liu et al., 2021; Wu et al., 2011).

After six decades of practices, approximately 70% of global cultivars carry one of these two alleles (Wurschum et al., 2017), and although they significantly altered plant structure related traits (Lanning et al., 2012; Sherman et al., 2014), their effects on wheat root remain largely unclear.

With the increase in sequencing accuracy, large-scale population transcriptome sequencing is becoming an option for SNP identification (Fu et al., 2013; Zhang et al., 2017). The transcriptional data also provide a link between the traits and the SNP variations, that cannot be readily captured at the sequence level (Azodi et al., 2020), thus providing an important bridge from DNA to phenotypes and critical clues for the investigation of underlying mechanisms of functional variations.

Here, we analyzed transcriptomes and phenotypes of seedlings roots of a natural bread wheat population, revealing that the modern wheat breeding selection substantially altered root transcriptomes and development. Our results demonstrated that *Rht-D1b* was the major allele that conferred large root systems to modern wheat cultivars. The population transcriptome and cytological analysis showed that *Rht-D1b* regulates a broad of genes involved in wheat root development, and increases the root cell width and root diameter, thereby significantly enhances the root-shoot ratio of modern wheat, which provides new insights for *Rht-D1b* application in futural wheat breeding practice.

RESULTS

A large-scale transcriptome sequencing reveals the gene composition and variations in wheat seedling root

A large-scale RNA-seq was performed on 406 worldwide bread wheat accessions (Table S1) with the seedling root samples at 14 days after germination (DAGs), producing 15.98 billion high-quality reads, and identifying 1,232,311 single nucleotide polymorphisms (SNPs) with an average density of 10 SNPs per gene (Fig. 1A). The accuracy of the identified SNP was validated as > 99% by wheat microarray evaluation, (Table S2). About half of the SNPs (48.43%) were located in CDS (coding

DNA sequence) regions (Fig. 1B), demonstrating a feature of the transcriptome derived SNPs.

With this population, 107,662 genes were identified as expressed gene in wheat root, including 39,243 wheat low confidence (LC) genes, extending the number of verified wheat genes in the current wheat genome. The expression levels of these genes ranged from 0.5 to 21,144.5 TPM (transcripts per million). The highly expressed genes were enriched in “response to water deprivation” and “water transport” (Fig. 1C and Table S3) pathways, highlighting the root function as the water uptake organ. Interestingly, the categories of “response to water deprivation” and “water transport” were also enriched in the highly varied expression genes in the natural population (Fig. 1D and Table S4), indicating that the water uptake processes may be highly varied among wheat cultivars.

Modern wheat breeding substantially altered the root transcriptome and development

Phylogenetic and population structure analyses clearly separated 190 modern cultivars (MC) and 87 landraces (LA) from the 406 wheat accessions (Fig. 2A and 2B). Then, 10,722 differentially expressed genes (DEGs) were identified between LA and MC groups (FDR-adjusted $P < 0.05$; Table S5).

GO enrichment analysis of the DEGs showed that the MC significantly changed in environmental stress response, development, and phytohormones signaling transductions (Fig. 2C and Table S6). Notably, the homologs of 41 DEGs in other plants were identified as the key genes involved in root development (Table S7), including *AtRCD1* (Teotia and Lamb, 2011), *AtARR10* (Yokoyama et al., 2007; Zubo et al., 2017), *AtEXPB2* (Wu et al., 2001), *OsSHB* (Li et al., 2015), *OsAUX3* (Wang et al., 2019) and *OsERF2* (Xiao et al., 2016), suggesting that the root development may be altered in MC. The population phenotypic investigation showed the root number, diameter, surface, and volume were significantly higher ($P < 0.01$) in the MC than LA groups at 14 DAGs (Fig. 2D), supporting the modern wheat breeding substantially altered root development.

Rht-D1b is the major allele that contributes a large root to modern wheat cultivars

With the population root phenotypes and SNP variations from transcriptome, the genome-wide association studies (GWAS) detected a quantitative trait locus (QTL) on 4D that was significantly associated ($P < 10^{-5}$) with root surface and volume, which contained the well-known *Rht-D1* and contributed to 17.1-25.2% variation of these traits (Fig. 3A and Table S8).

In population, the *Rht-D1b* genotypes had significantly higher values for total root length, diameter, surface, and volume than *Rht-D1a* genotypes (Fig. 3B). However, if the cultivars containing *Rht-D1b* were removed from MC group, the root surface and volume did not differ between LA and MC (i.e., comparison between LA and *Rht-D1a* MC) (Fig. 3B), strongly supporting the hypothesis that *Rht-D1b* is the major allele that altered the modern wheat root system.

Then, we argued that the earlier germination or the big grain size may also arise the conclusion of bigger root system in MC. Thus, the kernel weight was treated as fixed effects in a linear model to adjust the root phenotypes, and we found the root surface, root volume and root diameter still be significantly higher in accessions containing *Rht-D1b* (Fig. S1A), and the region of *Rht-D1b* still be the significantly Loci for root surface and volume in the GWAS analysis (Fig. S1B and Table S9), suggesting that *Rht-D1b* has a role in promoting root growth independent of the grain size. To judge the effect of the earlier germination on root development, the seedling root development was systematically and continuously investigated (Fig. 3C). At four DAGs, the root length was significantly shorter in the *Rht-D1b* than *Rht-D1a* genotypes. At seven DAGs, the *Rht-D1b* genotypes had significantly larger root diameters and volumes than *Rht-D1a* genotypes. The total root length and surface significantly increased until 14 DAGs (Fig. 3C). These observations suggest that the large roots of *Rht-D1b* are due to faster growth after germination rather than earlier germination.

Finally, the full CDS containing *Rht-D1b* allele driven by the *Rht-D1* promoter was cloned into wheat cv. Fielder (*Rht-D1a* and *Rht-B1b* background), and this

confirmed its role in increasing total root length, root diameter, and a large root system (Fig. 3D), supporting that the *Rht-D1b* has an important role in enlarging wheat root system.

The large root system of the *Rht-D1b* partially depends on the inhibition of GA signaling

Eight wheat accessions of each group of the *Rht-D1b*, *Rht-B1b,* and *Rht-B1aRht-D1*a (marked *NO*) were randomly selected (Table S10) to form of a sub-population, then treated by exogenous GA in a hydroponics system. The accessions containing *Rht-B1b* and *Rht-D1b* showed significantly increased in the number of roots, root surface and root volume than *NO* genotypes without GA treatment (Fig. 4A). With the exogenous GA treatment, these under-ground root traits were significantly inhibited in the *NO* group (Fig. 4A). Both cultivars containing *Rht-B1b* and *Rht-D1b* had lower sensitivities to exogenous GA treatments (Fig. 4A), although they displayed similar responsive trends with the *NO* group, suggesting that the GA signals plays a negative effect in wheat root development, which contribute the larger root system to cultivars containing *Rht-D1b* and *Rht-B1b*. Moreover, the *Rht-D1b* accessions showed higher GA insensitivity compared to *Rht-B1b* accessions, consistent to previous general conclusion, the *Rht-D1b* showed a stronger inhibited effect on GA signaling. Consistently, the *Rht-D1b* accessions showed higher value in root traits compared those in accessions containing *Rht-B1b*, further support that the suppressed GA signaling contribute the larger root system to wheat seedling, and implying the higher inhibited effect of *Rht-D1b* contribute the larger root system compared to *Rht-B1b*.

The same accessions were further treated by the exogenous auxin (NAA) and brassinosteroids (BL) with similar treatment procedure, the sensitivity to NAA (Fig. S2) and BL (Fig. S3) among the *NO*, *Rht-D1b*, and *Rht-B1b* didn't show stable and significant difference in these root traits, supporting that GA is the major phytohormone that altered root development in *Rht-B1b* and *Rht-D1b* cultivars.

Intriguingly, both GA treatment and *Rht-B1b* genotype did not significantly alter root diameters, indicating that the *Rht-D1b* allele may also have a GA-independent role in regulating root diameter.

However, the above-ground traits leaf and coleoptile length showed an increased in *NO* groups (Fig. 4B), and with the exogenous GA treatments the growth was further promoted (Fig. 4B). These observations suggested the GA confers an opposite effect on above- and under-ground tissue growth, and the large root system of *Rht-D1b* genotypes is related to GA signaling, as the typical semidwarf plant height conferred by the suppressed GA signaling (Rizza and Jones, 2019).

The increase of cell size underlies the larger root system of *Rht-D1b*

To clarify the underlying mechanism of *Rht-D1b* in regulating root development, the root meristem was investigated in *Rht-D1b* transgenic lines, showing the meristem length and width of *Rht-D1b* had significantly increased (Fig. 5B). Further cytological observation showed the cell width of *Rht-D1b* in the meristem zone had increased, which would be the reason for the larger meristem width. The number of cells in longitudinal meristems was significantly more than the wildtype, whereas the average cell length was similar to the wildtype. Since the half-length of cell width is used to define the meristem region, the increased number of dividing cells and meristem length may also be derived from the increased cell width. Indeed, for cells in the mature root region, both the cell length and width had increased (Fig. 5C), but keep similar ratio of length/width, highlighting the increased cell width in meristem plays critical role for increasing the size of root cells.

In contrast, the cell length of above-ground tissues was significantly decreased in length (Fig. 5D-F), consistent with their well-known dwarf phenotype, further supporting the distinct regulation pattern of GA signaling between above- and under-ground tissues.

Rht-D1b* regulates a broader gene network compared to *Rht-B1b

To characterize the underlying mechanism by which *Rht-D1b* regulates wheat root phenotypes, co-expression analysis was performed on the transcriptomic data. The genes co-expressed with *Rht-D1* were more than those co-expressed with *Rht-B1* in *NO* genotypes (Fig. 6A and Table S11). Besides, genes co-expressed with *Rht-D1* in *Rht-D1b* genotypes included almost all the genes co-expressed with *Rht-B1* in the *Rht-B1b* genotypes, supporting *Rht-D1* had a bigger gene co-expression network. Further analysis showed that the *Rht-D1* have 11,065 co-expressed genes in *Rht-D1b* genotypes out of the whole gene network of all three *Rhts* (Rht-A1a, B1a and D1a) in *NO* genotypes, whereas only 4,251 gene is co-expressed with *Rht-B1b* under this circumstance, further support that the *Rht-D1b* has a broader regulatory gene spectrum than *Rht-B1b*.

Consistently, the DEGs number caused by *Rht-D1b* is much more than that caused by *Rht-B1b* (Fig. 6B, Table S12 and Table S13), GO enrichment showed a broader influence by the *Rht-D1b* (Fig. 6C and Table S14), which contains several phytohormones and meristem development category, further supporting that the *Rht-D1b* have a broader genes network, and implying that *Rht-D1b* has more functions in regulating root development.

Interestingly, the two major wheat regions in China, the Yellow and Huai wheat production region (Y&H) and Yangtze River winter wheat production region (YR), had a distinct preference for these two alleles (Fig. 6D). Modern wheat cultivars in Y&H were predominantly *Rht-D1b*, whereas almost all YR cultivars were *Rht-B1b*, and this may be related to the root traits of these two alleles.

Opposing GA responses to above- and under-ground tissues contribute to a high root-shoot ratio

The opposing effects of GA on the above- and under-ground traits (Fig. 4 and 5) suggested a role of *Rht-B1b* and *Rht-D1b* in regulating wheat root-shoot ratio. To confirm this hypothesis, the fresh weight of shoots and roots at seven DAGs was investigated. The root-shoot ratio had significantly increased in *Rht-D1b* and *Rht-B1b* genotypes (Fig. 7A). GWAS identified *Rht-D1b* as the critical allele that increased the

root-shoot ratio of modern wheat cultivars (Fig. 7B and Table S15). *Rht-B1b* was also significantly associated with the high root-shoot ratio when *Rht-D1b* genotypes were removed from the population, suggesting a stronger effect of *Rht-D1b*, which masked that of *Rht-B1b*. The contribution and reliability of *Rht-D1b* associations with root-shoot ratios in GWAS clearly increased when the *Rht-B1b* genotypes were removed, indicating interferences from *Rht-B1b*. These results suggest that *Rht-D1b* and *Rht-B1b* significantly increased the root-shoot ratio at the early developmental stage and provided new insights for the successful utilization of these green revolution alleles.

Collectedly, the modification of modern wheat with *Rht-D1b* and *Rht-B1b* suppressed GA signaling, which conferred distinct responses between above- and under-ground tissues, increased the cell sizes in roots, but inhibited the cell length in above-ground tissues, conferring a large root system and a high root-shoot ratio to modern wheat cultivars (Fig. 7C). The *Rht-D1b* also have a role independent of GA signals to promote the root diameter, confers a stronger effect in enhancing wheat root systems and root-shoot ratios, which significantly altered root-related traits in current wheat cultivars.

DISCUSSION

In this study, the large-scale transcriptome sequencing data availed high-density SNP markers for subsequent gene evaluation. A total of 39,243 LC genes were identified in the wheat root, and this not only provided transcriptional evidence for LC genes but also expanded the wheat genome database. Based on analysis of identified SNP and wheat root phenotypes, *Rht-D1b* was identified as the major allele for enhancing root systems in modern wheat cultivars.

It has been suggested that targeting roots for crop improvement may be the solution to the second Green Revolution (Den Herder et al., 2010; Lynch, 2007). Although either an increased root length or number enlarged the root system, we found that the large root diameters conferred by the *Rht-D1b* allele were the major cause of large root volumes. This result enlightens a new direction for root

improvement by enhancing root cell width and root diameter, which may reconcile the competition between the length and number of roots (van der Bom et al., 2020) to form a large root system.

Bearing the *Rht-D1b* allele contributed to large seedling roots in modern wheat, and was preferentially adopted in the Y&H wheat production region The drought and cold winter ecology conditions in Y&H may be the important reason for *Rht-D1b* adoption here. It will be an interesting and important question to clarify the connections between the bigger root system and its geographic adoption in different wheat regions in China (Gao et al., 2015; Zhang et al., 2006), the USA (Guedira et al., 2010) and Europe (Wurschum et al., 2015; Wurschum et al., 2018).

Although gibberellins enhanced root cell elongation (Shani et al., 2013) and root meristem proliferation (Qin et al., 2022), it is the *Rht-D1b*-mediated increase in cell width that results in large root systems. Similarly, the cell length reduction is the major mechanism for the dwarf phenotypes, suggesting the critical role of GA in controlling plant cell shape. This diverged GA signaling responses between the above- and under-ground tissue is due to their distinct GA sensitivity (Tanimoto, 2012). The reduced GA production barely affected root growth. In contrast, over-production of GA inhibited root growth (Qin et al., 2022), consistent with that the root is very sensitive to GA and reaches the saturated status with low concentration maintenance (Tanimoto, 2012). In this study, both *Rht-B1b* and *Rht-D1b* genotypes showed a low sensitivity to GA treatment yet responded to the exogenous GA (Fig. 4A) to inhibit root growth, indicating that their root development benefited from the suppressed GA signaling. However, these findings suggest that GA signaling seems contribute a negative effect on root growth in *NO* genotype wheat which is contradicts to the previous conclusion that low GA concentration promoted root growth in most plant species (Tanimoto, 2012), thus, the underlying mechanism remains largely unknown.

In plants, the GA synthesis and transportation (Binenbaum et al., 2018; Topham et al., 2017) is a complex gene network. Moreover, the functions of GA in the plant are both spatial (Topham et al., 2017) and temporal dependent (Qin et al., 2022),

confounding our understanding of the regulatory mechanisms of *Rht-B1b* and *Rht-D1b*. Our findings that GA distinct affects between above- and under-ground tissues, *Rht-B1b* and *Rht-D1b* functions in enlarging both the root system and root-shoot ratio, and *Rht-B1b* and *Rht-D1b* encode different functions, are useful not only for research on the regulatory mechanisms of GA, but also wheat breeding and cultivation practices.

Materials and Methods

Plant materials and Root development trait measurement

The 406 bread wheat (*Triticum aestivum* L.) accessions used in this study included 87 landraces, 43 historical cultivars (the cultivars released before 1970), 190 modern cultivars (the cultivars released after 1970), and 60 breeding lines (Table S1). Similar size seeds were selected for each accession, and sterilized with 2% sodium hypochlorite for 10 min and then rinsed 3-5 times with distilled water. Then twenty sterilized seeds of each accession were incubated at 4 □ in darkness for 2 days to break dormancy. The germinated seeds of each accession were placed on damp filter papers in the germination box (12×12×5 cm) and cultivated under 22 □/16 □ day/night (50% relative air humidity) and 16 h light (2000 Lux) / 8 h dark cycles. After 14 days, seven highly similar robust seedling were collected for each accession, one seedling root were immediately frozen in liquid N2 for the subsequent RNA isolation, and other 6 samples were used for phenotyping total root length, root surface, root volume, and root diameter with the Wseen LA-S image system (Hangzhou Wseen Testing Technology Co. LTD), and manually measuring the number of roots and the primary root length. For each accession, six independent replications were performed, and produced 36 root sampling data and 6 independent samples for RNA preparation. The dynamic root development measurements were performed at 4 and 7 DAGs seedling with same procedure as above.

RNA sequencing and Reads mapping

Six independent samples from six replications (one root sample per replication)

were equally bulked for total RNA extraction, and the RNA-seq libraries generation in collaboration with Frasergen Bioinformatics Co., Ltd. (Wuhan, China). Briefly, the paired-end sequencing libraries with an insert size of ~250 bp were sequenced on the Illumina HiSeq X Ten platform. Using Trimmomatic (v0.33) (Bolger et al., 2014), raw reads were trimmed to remove sequencing adapters, and reads with low-quality bases were culled. Reads were then aligned to the bread wheat reference genome (IWGSC RefSeq v1.0) using the STAR software (v2.4.2a) (Dobin et al., 2013) in the 2-pass mapping mode. Reads were also mapped to the transcriptome sequence (IWGSC RefSeq v1.1 annotation) with BWA (v0.7.17) (Li and Durbin, 2010). Uniquely mapping reads that had the same mapping loci on both genome and transcriptome and the proper mapping distances with the relatively paired reads (< 63,068 bp based on the largest intron length in the whole genome) in the reference sequence alignment, were selected to reduce mapping errors and used for the subsequential SNP calling.

SNP calling and Annotation

A two-step procedure (Fu et al., 2013) were employed with a few of modifications. In details, the raw SNPs were called with a population SNP-calling manner referring to the best practices of GATK (v4.0.2.0) (McKenna et al., 2010). The “MarkDuplicates” module (Picard-2.17.11) was used to mark the duplication alignment, “SplitNCigarReads” module (GATK v4.0.2.0) was used to remove the sequences spanning intronic regions, and “HaplotypeCaller” module (GATK v4.0.2.0) was used to generate individual variants for each sample. SNPs were filtered with the following parameters: mapping quality ≥ 40, SNP quality ≥ 30, genotype quality for each accession ≥ 20, QD (SNP quality/reads depth) ≥ 2; each SNP was more than 5 bp away from an InDel; for homozygous genotypes, the supporting reads ≥ 5 for each accession; for heterozygous genotypes, the supporting reads for both the reference and alternative alleles ≥3 for each accession. SNPs that did not meet these parameters were termed missing. To further exclude possible false polymorphic sites caused by intrinsic mapping errors which mainly resulted from the homologous on the reference

genome and mapping bias inherent to the mapping algorithm, SNPs identified in the accession of wheat cv. Chinese Spring which was used to generate reference genome sequence, were defined as error-prone SNP sets. Any SNPs that matched the error-prone set were culled. The SNPs that met the filtering criteria were termed high-quality SNPs, and annotated using the SnpEff (v4.3) (Cingolani et al., 2012). This SNP calling pipeline could be downloaded from https://github.com/biozhp/Population_RNA-seq.

SNP validation

To evaluate and improve the reproducibility of the pipeline and the accuracy of the final SNPs, the accession of wheat cv. Chinese Spring as the positive transcriptome control (IWGSC RefSeq v1.1 annotation), there are only 387 alternative alleles (0.1%) were detected in this accession in population transcriptomic data, suggesting a low false-positive rate of our pipeline. Then, three accessions (s542, s543 and s544) with two biological replications were selected from the population for RNA-seq library construction and SNP identification. The results an average concordant rate of 98.85% between two-replication RNA samples and one RNA sample in population transcriptomic analysis, indicating that the SNP calling pipeline was highly reproducible (Table S16). At last, four accessions (K147, K95, s542 and s543) were selected to genotype with wheat 660□K SNP arrays, and the resultant accuracies were > 99% (Table S2). Thus, these results corroborated the accuracy and reliability of our SNP data. In turn, these validations provide key clues to improve the parameters in the pipeline.

SNP imputation

Beagle (v5.4) (Browning et al., 2018) was used to impute missing genotypes. All heterozygous genotypes were masked as missing genotypes before imputation. To get the optimal imputation accuracy and filling rate, 28,257 sites were randomly masked as missing, the missing rate varied from 10 to 90%, and were subsequently imputed using default parameters. The imputation accuracy was measured by determining the

proportion of correctly inferred genotypes from the total masked genotypes, and found that the imputation accuracy was more than 99% when the missing rate was < 0.8 (Table S17). By combining imputation accuracies and filling rates, SNPs with a missing rate < 0.8 were imputed.

Phylogenetic analysis

RAxML (v8.2.12) (Stamatakis, 2014) was used to construct a maximum-likelihood tree using imputed SNPs of MAF > 0.2, and the command "-f a -m GTRGAMMA -p 12346 -x 12346 -# 100". The phylogenetic tree was visualized in iTOL (v6) (Letunic and Bork, 2021). Imputed SNPs with MAF > 0.05 were used to quantify and infer population structures in ADMIXTURE (v1.3.0) (Alexander et al., 2009). The parameters K = 2 -10 were used to identify different groups, and finally K = 4 was used in subsequent analysis.

Quantification of gene expression

Reads were aligned to high and low confidence transcripts (IWGSC RefSeq v1.1 annotation) with the default parameters in Kallisto (v0.46.2) (Bray et al., 2016). The transcript expression values (Transcripts Per Million, TPM) were summarized to gene expression levels using R package Tximport (v1.14.0) (Soneson et al., 2015) with the "lengthScaledTPM" option (Ramirez-Gonzalez et al., 2018). To investigate the extent of gene expression variation within the population, genes with TPM > 0.5 in at least 5% of accessions (20 accessions) were selected, and the fold change of their TPM at 95th percentiles to that of the 5th percentiles (TPM > 0.5) in the whole population was calculated.

Identification of differentially expressed genes (DEGs)

Linear mixed model (Ku et al., 2021) was performed in DEGs identification for its superior sensitivity in controlling the confounders:

$$y = \mu + X\alpha + P\beta + K\gamma + e$$

In this equation, y represents the expression values (TPM) of the compared gene among the whole population, μ represents is the overall mean, X represents the two

groups, between of which the gene expression levels were compared, P is the PCA matrix and K is the relative kinship matrix. $X\alpha$ and $P\beta$ represent fixed effects, and $K\gamma$ represent random effects. The PCA matrix and kinship matrix were generated with GAPIT (v3.1) (Wang and Zhang, 2021). The top three principal components were used to build up the P matrix for population-structure correction. The K matrix was used to correct the potential familial relatedness. Analysis was performed with R using the package lmerTest (v3.1-3). The significance (P-value) of the $X\alpha$ was extracted using the "anova" function and was used to indicate whether the expression levels of target gene were significantly different between the two compared groups. The P-values were adjusted for multiple testing by controlling for FDR with the BH method and the genes with FDR adjusted P-value < 0.05 were considered as candidate DEGs. To exclude the random error from the single sample RNA-seq, only genes detected in 20 accessions at least were applied with the DEGs analysis, and all DEGs identified with the groups pairs in which each group contains more than 20 accessions at least (5% of population, presenting 20 replications for any given genotype).

GO enrichment analysis

GO annotations of high confidence genes were downloaded from the Ensembl Plants Genes 53 database, and GO annotations of low confidence genes were obtained with eggNOG-mapper (v2) (Cantalapiedra et al., 2021). GO enrichment analysis was performed using the R package clusterProfiler (v3.18.1) with the “enricher” function (Yu et al., 2012). The P-values were adjusted for multiple testing with the procedure of Benjamini and Hochberg.

Genome-wide association analyses

The GWAS analysis with the mixed linear model (PCA + kinship) implemented in GAPIT (v3.1) (Wang and Zhang, 2021) was applied on the imputed SNPs with MAF > 0.05. The PCA and kinship matrix were generated using GAPIT with the default parameters to correct the population structure and familial relatedness,

respectively. A Bonferroni-corrected threshold probability based on individual tests was calculated to correct for multiple comparisons using 0.05/N, where N is the effective SNP number calculated with the Genetic type 1 Error Calculator (v0.2). The significant *P-value* thresholds for root surface and volume were 4.29×10^{-5}. Those for root-shoot ratio were 4.46×10^{-5}, 4.52×10^{-5}, and 4.36×10^{-5} for the whole population and the sub-populations removing either *Rht-B1b* or *Rht-D1b* genotypes, respectively. The kernel weight was treated as fixed effects in a linear model to adjust the data of root phenotypes with the "lm" function in R (v 3.6.1) (Chambers and Hastie, 1992), and the adjust root phenotypic data was further applied into the genetic effect analysis and GWAS analysis.

Permutations of the phenotyping comparison

To minimize false positive errors, the 1,000 permutation tests (Zhou et al., 2020) were conducted in phenotyping comparison. In each permutation test, 60% of accessions were randomly sampled from each of the two compared groups and the significance level of the differences of target trait between the two sampled groups were calculated using Student's t-tests. The total number of significant differences (P-value < 0.01) in the 1,000 permutation tests was recorded.

Identification of genes co-expressed with *Rht-A1/B1/D1*

Genes co-expressed with *Rht-A1/B1/D1* were identified with the Gini correlation coefficient (GCC) algorithm (Ma and Wang, 2012). The Gini correlation coefficient (GCC) values calculated by the R package rsgcc (v1.0.6), and the gene pairs with the |GCC| value ≥0.5 and *P-value* < 0.01 were considered as co-expressed genes.

Hormone treatment

Eight randomly selected accessions (Table S10) from each group of the *Rht-B1aRht-D1a*, *Rht-B1bRht-D1a*, and *Rht-B1aRht-D1b*, and were treated with 0.2 μM and 2 μM gibberellic acid (GA3), 10 nM and 100 nM Epibrassinolide (EpiBL), 50 nM and 500 nM 1-Naphthaleneacetic acid (NAA). Control plants for GA3, EpiBL,

and NAA were treated with mock solutions of distilled water containing ethanol, DMSO, and ethanol, respectively. The sterilized seeds (highly similar size seeds were selected for each accession) were incubated in the dark at 4 °C for two days and then cultivated in a germinating box for one day, then treatment with hormones until 14 DAGs. For each accession, three independent replications were conducted for each treatment, and at least six plants were used for each replication.

Over-expression transgenic vector construction and plant transformation

The cDNA of *TaRht-D1b* was cloned (1872 bp from wheat cv. Kenong199) and transferred into the pMWB111 vector with *TaRht-D1* native promoter (1876 bp from wheat cv. Kenong199), then transformed into wheat cv. Fielder using *Agrobacterium tumefaciens*-mediated transformation (Hayta et al., 2019). All transgenic lines were confirmed by PCR and sequencing. To reduce different grain weight interferes on root development, similar size seeds from transgenic lines and wild type were selected for phenotyping.

Cytological observation of roots and shoots

Confocal laser scanning microscopy (CLSM) was used for cytological observations of roots and shoots. CLSM samples were prepared according to previous report (Wang et al., 2021). Samples were harvested and fixed in 4% glutaraldehyde (in 12.5 mM cacodylate, pH 6.9), desiccated in vacuo for 30 min, after which they were incubated overnight in a fixative at room temperature. After fixation, tissues were dehydrated through different gradients of ethanol absolute (50%, 60%, 70%, 85%, 95% and 100% ethanol absolute) for 30 min per step. Then, tissues were clarified with 2:1 (v/v) benzyl benzoate: benzyl alcohol for a minimum of 1 h. Samples were observed under a confocal microscope coupled to a 488-nm argon laser (Olympus, Fluoview1200, Tokyo, Japan). ImageJ (v1.48) software was used to measure the length and width of the cell.

Data availability

The raw RNA-Seq data were deposited in the Sequence Read Archive (https://www.ncbi.nlm.nih.gov/sra) under accession numbers PRJNA838764. Genotypic, transcriptomic and phenotypic data used in this analysis are publicly available from our website (https://iwheat.net/resource/). All the code of analysis could be downloaded from https://github.com/biozhp/Population_RNA-seq.

FUNDING

This work was supported by grants from the National Natural Science Foundation of China (31571756 and 31870298) to S.X., the fellowship of China Postdoctoral Science Foundation (2021T140566) to X.W.

AUTHOR CONTRIBUTIONS

S.X. and Z.K. conceived the project and designed the research. Z.K., S.X. and D.H. collected wheat accession. X.W., P.Z., X.G., Z.L., X.M., Y.Z., X.L., L.H. and W.W. performed the sample preparation, RNA sequencing and phenotypic data collection and process. S.X., X.W., P.Z., X.G. organized the data and wrote the manuscript. All authors discussed the results and commented on the manuscript. All authors read and approved the final manuscript.

ACKNOWLEDGEMENTS

We thank the Weining Song, Xinhong Chen and Hude Mao for helping in germplasm collection, Xueyong Zhang and Zhongfu Ni give the valuable suggestions for this study, the computing platform support of High-Performance Computing of NWAFU.

REFERENCES

Abbo, S., van-Oss, R.P., Gopher, A., Saranga, Y., Ofner, I., and Peleg, Z. (2014). Plant domestication versus crop evolution: a conceptual framework for cereals and grain legumes. Trends in plant science **19**:351-360.

Alexander, D.H., Novembre, J., and Lange, K. (2009). Fast model-based estimation of ancestry in unrelated individuals. Genome Res **19**:1655-1664.

Azodi, C.B., Pardo, J., VanBuren, R., de Los Campos, G., and Shiu, S.H. (2020). Transcriptome-Based Prediction of Complex Traits in Maize. Plant Cell **32**:139-151.

Bacher, H., Zhu, F., Gao, T., Liu, K., Dhatt, B.K., Awada, T., Zhang, C., Distelfeld, A., Yu, H., Peleg, Z., et al. (2021). Wild emmer introgression alters root-to-shoot growth dynamics in durum wheat in response to water stress. Plant Physiol **187**:1149-1162.

Binenbaum, J., Weinstain, R., and Shani, E. (2018). Gibberellin Localization and Transport in Plants. Trends Plant Sci **23**:410-421.

Bolger, A.M., Lohse, M., and Usadel, B. (2014). Trimmomatic: a flexible trimmer for Illumina sequence data. Bioinformatics **30**:2114-2120.

Bray, N.L., Pimentel, H., Melsted, P., and Pachter, L. (2016). Near-optimal probabilistic RNA-seq quantification. Nat Biotechnol **34**:525-527.

Browning, B.L., Zhou, Y., and Browning, S.R. (2018). A One-Penny Imputed Genome from Next-Generation Reference Panels. Am J Hum Genet **103**:338-348.

Calleja-Cabrera, J., Boter, M., Oñate-Sánchez, L., and Pernas, M. (2020). Root Growth Adaptation to Climate Change in Crops. Front Plant Sci **11**:544.

Cantalapiedra, C.P., Hernandez-Plaza, A., Letunic, I., Bork, P., and Huerta-Cepas, J. (2021). eggNOG-mapper v2: Functional Annotation, Orthology Assignments, and Domain Prediction at the Metagenomic Scale. Mol Biol Evol **38**:5825-5829.

Chambers, J., and Hastie, T. (1992). Linear models. Chapter 4 of statistical models in S. Wadsworth & Brooks/Cole **1992**.

Cingolani, P., Platts, A., Wang le, L., Coon, M., Nguyen, T., Wang, L., Land, S.J., Lu, X., and Ruden, D.M. (2012). A program for annotating and predicting the effects

of single nucleotide polymorphisms, SnpEff: SNPs in the genome of Drosophila melanogaster strain w1118; iso-2; iso-3. Fly (Austin) **6**:80-92.

D'Alessandro, S., Golin, S., Hardtke, C.S., Lo Schiavo, F., and Zottini, M. (2015). The co-chaperone p23 controls root development through the modulation of auxin distribution in the Arabidopsis root meristem. J Exp Bot **66**:5113-5122.

de Vries, F.T., Griffiths, R.I., Knight, C.G., Nicolitch, O., and Williams, A. (2020). Harnessing rhizosphere microbiomes for drought-resilient crop production. Science **368**:270-274.

Den Herder, G., Van Isterdael, G., Beeckman, T., and De Smet, I. (2010). The roots of a new green revolution. Trends Plant Sci **15**:600-607.

Dobin, A., Davis, C.A., Schlesinger, F., Drenkow, J., Zaleski, C., Jha, S., Batut, P., Chaisson, M., and Gingeras, T.R. (2013). STAR: ultrafast universal RNA-seq aligner. Bioinformatics **29**:15-21.

Fu, J., Cheng, Y., Linghu, J., Yang, X., Kang, L., Zhang, Z., Zhang, J., He, C., Du, X., Peng, Z., et al. (2013). RNA sequencing reveals the complex regulatory network in the maize kernel. Nat Commun **4**:2832.

Gao, Z., Shi, Z., Zhang, A., and Guo, J. (2015). Distribution of genes associated with yield potential and water-saving in Chinese Zone II wheat detected by developed functional markers. Journal of genetics **94**:35-42.

Godfray, H.C., Beddington, J.R., Crute, I.R., Haddad, L., Lawrence, D., Muir, J.F., Pretty, J., Robinson, S., Thomas, S.M., and Toulmin, C. (2010). Food security: the challenge of feeding 9 billion people. Science **327**:812-818.

Golan, G., Hendel, E., Méndez Espitia, G.E., Schwartz, N., and Peleg, Z. (2018). Activation of seminal root primordia during wheat domestication reveals underlying mechanisms of plant resilience. Plant Cell Environ **41**:755-766.

Guedira, M., Brown-Guedira, G., Van Sanford, D., Sneller, C., Souza, E., and Marshall, D. (2010). Distribution of Rht Genes in Modern and Historic Winter Wheat Cultivars from the Eastern and Central USA. Crop Science **50**.

Hao, C., Jiao, C., Hou, J., Li, T., Liu, H., Wang, Y., Zheng, J., Liu, H., Bi, Z., Xu, F., et al. (2020). Resequencing of 145 Landmark Cultivars Reveals Asymmetric

Sub-genome Selection and Strong Founder Genotype Effects on Wheat Breeding in China. Mol Plant **13**:1733-1751.

Hayta, S., Smedley, M.A., Demir, S.U., Blundell, R., Hinchliffe, A., Atkinson, N., and Harwood, W.A. (2019). An efficient and reproducible Agrobacterium-mediated transformation method for hexaploid wheat (Triticum aestivum L.). Plant Methods **15**:121.

Hendel, E., Bacher, H., Oksenberg, A., Walia, H., Schwartz, N., and Peleg, Z. (2021). Deciphering the genetic basis of wheat seminal root anatomy uncovers ancestral axial conductance alleles. Plant Cell Environ **44**:1921-1934.

Hou, L., Zhang, A., Wang, R., Zhao, P., Zhang, D., Jiang, Y., Diddugodage, C.J., Wang, X., Ni, Z., and Xu, S. (2019). Brassinosteroid Regulates Root Development with Highly Redundant Genes in Hexaploid Wheat. Plant & cell physiology **60**:1761-1777.

Hu, Y., Chen, J., Fang, L., Zhang, Z., Ma, W., Niu, Y., Ju, L., Deng, J., Zhao, T., Lian, J., et al. (2019). Gossypium barbadense and Gossypium hirsutum genomes provide insights into the origin and evolution of allotetraploid cotton. Nat Genet **51**:739-748.

IWGSC. (2018). Shifting the limits in wheat research and breeding using a fully annotated reference genome. Science **361**.

Khan, M.A., Gemenet, D.C., and Villordon, A. (2016). Root System Architecture and Abiotic Stress Tolerance: Current Knowledge in Root and Tuber Crops. Front Plant Sci **7**:1584.

Ku, A.T., Wilkinson, S., and Sowalsky, A.G. (2021). Comparison of approaches to transcriptomic analysis in multi-sampled tumors. Briefings in Bioinformatics **22**:bbab337.

Lanning, S.P., Martin, J.M., Stougaard, R.N., Guillen-Portal, F.R., and Talbert, L.E. (2012). Evaluation of Near-Isogenic Lines for Three Height-Reducing Genes in Hard Red Spring Wheat. Crop Science **52**:1145.

Lee, B.H., Ko, J.H., Lee, S., Lee, Y., Pak, J.H., and Kim, J.H. (2009). The Arabidopsis GRF-INTERACTING FACTOR gene family performs an overlapping

function in determining organ size as well as multiple developmental properties. Plant Physiol **151**:655-668.

Letunic, I., and Bork, P. (2021). Interactive Tree Of Life (iTOL) v5: an online tool for phylogenetic tree display and annotation. Nucleic Acids Res.

Li, H., and Durbin, R. (2010). Fast and accurate long-read alignment with Burrows-Wheeler transform. Bioinformatics **26**:589-595.

Li, J., Zhao, Y., Chu, H., Wang, L., Fu, Y., Liu, P., Upadhyaya, N., Chen, C., Mou, T., and Feng, Y. (2015). SHOEBOX modulates root meristem size in rice through dose-dependent effects of gibberellins on cell elongation and proliferation. PLoS Genetics **11**:e1005464.

Liu, Q., Wu, K., Harberd, N.P., and Fu, X. (2021). Green Revolution DELLAs: From translational reinitiation to future sustainable agriculture. Mol Plant **14**:547-549.

Lynch, J. (1995). Root Architecture and Plant Productivity. Plant Physiol **109**:7-13.

Lynch, J.P. (2007). Roots of the Second Green Revolution. Australian Journal of Botany **55**:493-512.

Ma, C., and Wang, X. (2012). Application of the Gini correlation coefficient to infer regulatory relationships in transcriptome analysis. Plant physiology **160**:192-203.

McKenna, A., Hanna, M., Banks, E., Sivachenko, A., Cibulskis, K., Kernytsky, A., Garimella, K., Altshuler, D., Gabriel, S., Daly, M., et al. (2010). The Genome Analysis Toolkit: a MapReduce framework for analyzing next-generation DNA sequencing data. Genome Res **20**:1297-1303.

Pearce, S., Saville, R., Vaughan, S.P., Chandler, P.M., Wilhelm, E.P., Sparks, C.A., Al-Kaff, N., Korolev, A., Boulton, M.I., Phillips, A.L., et al. (2011). Molecular characterization of Rht-1 dwarfing genes in hexaploid wheat. Plant Physiol **157**:1820-1831.

Qin, H., Pandey, B.K., Li, Y., Huang, G., Wang, J., Quan, R., Zhou, J., Zhou, Y., Miao, Y., Zhang, D., et al. (2022). Orchestration of ethylene and gibberellin signals determines primary root elongation in rice. Plant Cell **34**:1273-1288.

Ramirez-Gonzalez, R.H., Borrill, P., Lang, D., Harrington, S.A., Brinton, J., Venturini, L., Davey, M., Jacobs, J., van Ex, F., Pasha, A., et al. (2018). The

transcriptional landscape of polyploid wheat. Science **361**.

Rizza, A., and Jones, A.M. (2019). The makings of a gradient: spatiotemporal distribution of gibberellins in plant development. Curr Opin Plant Biol **47**:9-15.

Shani, E., Weinstain, R., Zhang, Y., Castillejo, C., Kaiserli, E., Chory, J., Tsien, R.Y., and Estelle, M. (2013). Gibberellins accumulate in the elongating endodermal cells of Arabidopsis root. Proceedings of the National Academy of Sciences of the United States of America **110**:4834-4839.

Sherman, J.D., Nash, D., Lanning, S.P., Martin, J.M., Blake, N.K., Morris, C.F., and Talbert, L.E. (2014). Genetics of End-Use Quality Differences between a Modern and Historical Spring Wheat. Crop Science **54**:1972-1980.

Snowdon, R.J., Wittkop, B., Chen, T.W., and Stahl, A. (2020). Crop adaptation to climate change as a consequence of long-term breeding. Theor Appl Genet.

Soneson, C., Love, M.I., and Robinson, M.D. (2015). Differential analyses for RNA-seq: transcript-level estimates improve gene-level inferences. F1000Res **4**:1521.

Stamatakis, A. (2014). RAxML version 8: a tool for phylogenetic analysis and post-analysis of large phylogenies. Bioinformatics **30**:1312-1313.

Tanimoto, E. (2012). Tall or short? Slender or thick? A plant strategy for regulating elongation growth of roots by low concentrations of gibberellin. Ann Bot **110**:373-381.

Teotia, S., and Lamb, R.S. (2011). RCD1 and SRO1 are necessary to maintain meristematic fate in Arabidopsis thaliana. J Exp Bot **62**:1271-1284.

Topham, A.T., Taylor, R.E., Yan, D., Nambara, E., Johnston, I.G., and Bassel, G.W. (2017). Temperature variability is integrated by a spatially embedded decision-making center to break dormancy in Arabidopsis seeds. Proceedings of the National Academy of Sciences of the United States of America **114**:6629-6634.

Van De Velde, K., Thomas, S.G., Heyse, F., Kaspar, R., Van Der Straeten, D., and Rohde, A. (2021). N-terminal truncated RHT-1 proteins generated by translational reinitiation cause semi-dwarfing of wheat Green Revolution alleles. Mol Plant **14**:679-687.

van de Wouw, M., van Hintum, T., Kik, C., van Treuren, R., and Visser, B. (2010).

Genetic diversity trends in twentieth century crop cultivars: a meta analysis. Theor Appl Genet **120**:1241-1252.

van der Bom, F.J.T., Williams, A., and Bell, M.J. (2020). Root architecture for improved resource capture: trade-offs in complex environments. J Exp Bot **71**:5752-5763.

Wang, J., and Zhang, Z. (2021). GAPIT Version 3: Boosting Power and Accuracy for Genomic Association and Prediction. Genomics Proteomics Bioinformatics **19**:629-640.

Wang, J., Guo, X., Xiao, Q., Zhu, J., Cheung, A.Y., Yuan, L., Vierling, E., and Xu, S. (2021). Auxin efflux controls orderly nucellar degeneration and expansion of the female gametophyte in Arabidopsis. New Phytologist **230**:2261-2274.

Wang, M., Qiao, J., Yu, C., Chen, H., Sun, C., Huang, L., Li, C., Geisler, M., Qian, Q., and Jiang, D.A. (2019). The auxin influx carrier, OsAUX3, regulates rice root development and responses to aluminium stress. Plant, Cell & Environment **42**:1125-1138.

Watt, M., Magee, L.J., and McCully, M.E. (2008). Types, structure and potential for axial water flow in the deepest roots of field-grown cereals. New Phytologist **178**:135-146.

Wu, J., Kong, X., Wan, J., Liu, X., Zhang, X., Guo, X., Zhou, R., Zhao, G., Jing, R., Fu, X., et al. (2011). Dominant and pleiotropic effects of a GAI gene in wheat results from a lack of interaction between DELLA and GID1. Plant Physiol **157**:2120-2130.

Wu, Y., Thorne, E.T., Sharp, R.E., and Cosgrove, D.J. (2001). Modification of expansin transcript levels in the maize primary root at low water potentials. Plant Physiol **126**:1471-1479.

Wurschum, T., Langer, S.M., and Longin, C.F. (2015). Genetic control of plant height in European winter wheat cultivars. Theor Appl Genet **128**:865-874.

Wurschum, T., Langer, S.M., Longin, C.F.H., Tucker, M.R., and Leiser, W.L. (2017). A modern Green Revolution gene for reduced height in wheat. Plant J **92**:892-903.

Wurschum, T., Liu, G., Boeven, P.H.G., Longin, C.F.H., Mirdita, V., Kazman, E., Zhao, Y., and Reif, J.C. (2018). Exploiting the Rht portfolio for hybrid wheat breeding. Theor Appl Genet **131**:1433-1442.

Xiao, G., Qin, H., Zhou, J., Quan, R., Lu, X., Huang, R., and Zhang, H. (2016). OsERF2 controls rice root growth and hormone responses through tuning expression of key genes involved in hormone signaling and sucrose metabolism. Plant molecular biology **90**:293-302.

Yokoyama, A., Yamashino, T., Amano, Y., Tajima, Y., Imamura, A., Sakakibara, H., and Mizuno, T. (2007). Type-B ARR transcription factors, ARR10 and ARR12, are implicated in cytokinin-mediated regulation of protoxylem differentiation in roots of Arabidopsis thaliana. Plant & cell physiology **48**:84-96.

Yu, G., Wang, L.G., Han, Y., and He, Q.Y. (2012). clusterProfiler: an R package for comparing biological themes among gene clusters. OMICS **16**:284-287.

Zhang, L., Su, W., Tao, R., Zhang, W., Chen, J., Wu, P., Yan, C., Jia, Y., Larkin, R.M., Lavelle, D., et al. (2017). RNA sequencing provides insights into the evolution of lettuce and the regulation of flavonoid biosynthesis. Nat Commun **8**:2264.

Zhang, X., Yang, S., Zhou, Y., He, Z., and Xia, X. (2006). Distribution of the Rht-B1b, Rht-D1b and Rht8 reduced height genes in autumn-sown Chinese wheats detected by molecular markers. Euphytica **152**:109-116.

Zhou, Y., Zhao, X., Li, Y., Xu, J., Bi, A., Kang, L., Xu, D., Chen, H., Wang, Y., Wang, Y.G., et al. (2020). Triticum population sequencing provides insights into wheat adaptation. Nat Genet **52**:1412-1422.

Zubo, Y.O., Blakley, I.C., Yamburenko, M.V., Worthen, J.M., Street, I.H., Franco-Zorrilla, J.M., Zhang, W., Hill, K., Raines, T., Solano, R., et al. (2017). Cytokinin induces genome-wide binding of the type-B response regulator ARR10 to regulate growth and development in Arabidopsis. Proc Natl Acad Sci U S A **114**:E5995-E6004.

Figure legends

Figure 1. The character of population transcriptome in wheat root.

(A) The distribution of the identified SNPs in wheat genome. The color indicates the number of SNPs within a window size of 1 Mb. **(B)** The distribution of the identified SNPs in gene regions. “UP” and “DOWN” represent the up- and down-stream 5 Kb regions that flank the annotated genes. **(C)** GO enrichment of the genes with highly and lowly expressed in seedling root. The 5% genes with highest expression (High_E) and lowest expression (Low_E) in population transcriptome were selected for this analysis. **(D)** GO enrichment of the genes with highly and lowly variations in expression levels. Genes with highly variations, High_V (fold change from > 8). Genes with lowly variations, Low_V (fold change from < 2).

Figure 2. The alterations of root transcriptome and root development in modern wheat cultivars.

(A) The phylogenetic tree of 406 wheat accessions. The phylogenetic tree was constructed and visualized with RAxML (v8.2.12) and iTOL (v6), respectively. Different color lines represent different groups. LA: landraces (red); HC: historical cultivars (green); MC: modern cultivars (blue); BL: breeding lines (orange). **(B)** Population structure of 406 wheat accessions with K = 2, 3, and 4. Matrices of membership coefficients of accessions corresponding to 2 - 4 hypothetical subpopulations derived from the structure analysis (ADMIXTURE v1.3.0). Each line represents a single accession. **(C)** GO enrichment of the differentially expressed genes (DEGs) between LA and MC groups. “UP” and “DOWN” represent the enriched categories of up- and down-regulated DEGs in MC group, respectively. **(D)** The comparisons of root phenotypes between LA and MC. The data was acquired from seedling at 14 days after germination (DAGs). Data are means ± SD, 36 samples for six replications were measured for each accession, and the average data of each accession was used for this comparison. Red numbers indicate the *P*-value from Student's *t*-tests, and “NS” refer no significance detected at $P < 0.01$ level. Black

numbers indicate the observed number with significant or insignificant difference in 1,000 permutations.

Figure 3. The Rht-D1b contributes a larger seedling root system to modern wheat cultivars.

(A) Genome-wide association analysis on root surface and volume. The phenotypic data was acquired and performed as Figure 2D. The number indicates the phenotypic variance explained by *Rht-D1b*. **(B)** The comparisons of root phenotypes between LA and MC at 14 DAGs. *Rht-D1a* and *Rht-D1b* refer the accessions of MC with *Rht-D1a* and *Rht-D1b*, respectively. Red numbers indicate the *P*-value from Student's *t*-test, and "NS" refer not significance detected at $P < 0.01$ level. Black numbers indicate the observed number with significant or insignificant differences in 1,000 permutations. **(C)** The comparisons of root phenotypes between *Rht-D1a* and *Rht-D1b* group at 4, 7, and 14 DAGs. **(D)** Root phenotypes of the *Rht-D1b* transgenic lines. The *Rht-D1b* was transformed into *Rht-B1b* background (wheat cv. fielder) driven by native *Rht-D1* promoter. WT, wild type (cv. fielder). D1 and D2, the transgenic line. Left panel is the phenotypes at 14 DAGs. Bar = 2 cm. Right panel presents the statistical data of the phenotypes. Data are means ± SD, 18 seedlings at least from three independent sample preparations were counted for each genotype. "*" and "**" indicate Student's *t*-test $P < 0.05$ and 0.01, respectively.

Figure 4. The effects of Rht-D1b on root development partly depend on GA signaling.

(A) The root phenotypes of different genotype with and without exogenous GA treatment. The indicated concentrations of GA were applied on the seedlings from 1 to 14 DAGs. Left part of each panel present the phenotypic data without GA treatment, and right part of each panel present the ratio of treated group phenotypic data to the average of untreated group phenotypic data within the same genotype. Data are means ± SD. Each genotype contained eight randomly selected accessions, at least six seedlings were counted for each accession, and replicate three times. *NO*

refers *Rht-B1aRht-D1a*, *B1b* refers *Rht-B1bRht-D1a* and *D1b* refer *Rht-B1aRht-D1b*. "*" indicates significant differences (Student's *t*-test $P < 0.01$) between with and without GA treatment. Different letters (a, b, and c) on the top indicate significant differences ($P < 0.01$) between different genotypes with multiple comparisons in a treated group by least significant difference (LSD) test. **(B)** The above-ground phenotypes of different genotype with and without GA treatment. The statistical data as described in (A).

Figure 5. Rht-D1b enlarges the cell size of roots but reduces the cell length in above-ground tissue.

CLSM records the cell morphology and size of above- and under-ground tissues in WT and *Rht-D1b* transgenic lines. WT, the control wheat cultivar Fielder, the D1 and D2 are different transgenic line of *Rht-D1b*. Seven samples were observed for each genotype, and at least 30 clear cells in each sample were measured with ImageJ software (v1.48). "*" in each panel indicates Student's *t*-test *P*-value < 0.05. **(A)** Diagram of the positions for microscopic observation. **(B)** Cells of root meristem. The average of seven samples were present in the figure and statistics. "Length" and "Width" represent the meristem length (indicated by Red dotted line) and meristem width (indicated by yellow dotted line), respectively. The cell length, cell number, and cell width were measured from the cell layer indicated by the red asterisk in left picture. Bar = 100 μm. **(C)** Cells of root maturation zone. "L1" and "L2" represent different cell layer indicated by the red and yellow dotted line, respectively. Bar = 200 μm. **(D)** Cells of leaf at the top part. Bar = 100 μm. **(E)** Cells of the leaf at the base part. Bar = 100 μm. **(F)** Cells of the coleoptile. Bar = 100 μm.

Figure 6. Rht-D1b had a broader regulatory gene spectrum.

(A) Venn diagrams depicting the overlap of genes co-expressed with *Rht-A1*, *Rht-B1*, and *Rht-D1*. The first Venn diagram indicates the genes co-expressed with three *Rhts* in the "NO" genotypic group (accessions with *Rht-B1aRht-D1a*). "*Rht-B1b*" indicates genes co-expressed with *Rht-B1* in "B1b" genotypic group (accessions with

Rht-B1bRht-D1a). "*Rht-D1b*" indicates genes co-expressed with *Rht-D1* in "D1b" genotypic group (accessions with *Rht-B1aRht-D1b*), and "Total" indicates the union genes which co-expressed with three *Rhts* in "NO" genotypic group. The group of "NO", "B1b" and "D1b" contained 200, 107 and 98 accessions, respectively. **(B)** The numbers of DEGs caused by *Rht-B1b* and *Rht-D1b* compared to "NO" groups under different significant level. The X-axis presents FDR adjust *P-value*. **(C)** GO enrichment of the DEGs under $P < 0.05$ and 0.01 standard in (B). **(D)** Distribution of MC with or without *Rht-B1b* and *Rht-D1b* alleles in Yangtze River (YR) and Yellow and Huai (Y&H) winter wheat production regions.

Figure 7. Rht-D1b increases the root-shoot ratio of wheat.

(A) The comparisons of root weight, leaf weight and root-shoot ratio in different genotypic group. NO refers *Rht-B1aRht-D1a*, B1b refers *Rht-B1bRht-D1a*, D1b refers *Rht-B1aRht-D1b*. The data was acquired from seedling at 7 DAGs of 344 accessions, 36 samples from six replications were measured for each accession, and the average data of each accession was used for this comparison. Red numbers indicate the *P-value* from Student's *t*-tests, and "NS" refer not significance detected at $P < 0.01$ level. Black numbers indicate the observed number of significant or insignificant differences in 1,000 permutations. **(B)** Genome-wide association analysis on root-shoot ratio. The phenotypic data was acquired and performed as (A). The number indicates the phenotypic variance explained by *Rht-D1b* or *Rht-B1b*. "Total", "NO B1b", and "NO D1b" indicate the whole populations, populations removed accessions with *Rht-B1b* and *Rht-D1b*, respectively. **(C)** Model diagram of *Rht-D1b* and *Rht-B1b* regulating wheat seedling development. The introduction of *Rht-D1b* and *Rht-B1b* suppressed the GA signaling, which conferred distinct GA responses between above- and under-ground tissues. They increased the cell length in the root and decreased the cell length in above-ground tissues. *Rht-D1b* also directly promoted the root diameter independent of GA signaling, resulting in a large root system and a high root-shoot ratio.

Figure S1. Root phenotype analysis after removing the influence of thousand kernel weight.

(A) The comparisons of adjusted root phenotypes between LA and MC at14 DAGs. *Rht-D1a* and *Rht-D1b* refer the accessions of MC with *Rht-D1a* and *Rht-D1b*, respectively. The adjusted root phenotypes are correcting potential effects of thousand kernel weight (TKW) on the root phenotypes with a linear model (R v3.6.1). Red numbers indicate the *P*-value from Student's *t*-test, and "NS" refer no significance detected at $P < 0.01$ level. Black numbers indicate the observed number of significant or insignificant differences in 1,000 permutations. **(B)** Genome-wide association analysis on adjusted root surface and volume at 14 DAGs. The phenotypic data was acquired and performed as (A). *P-value* threshold is 1/N, N represent the effective SNP number.

Figure S2. The above- and under-ground phenotypes of different genotype with and without exogenous NAA treatment.

The indicated concentrations of NAA were applied on the seedlings from 1 to 14 DAGs. Left part of each panel present the phenotypic data without NAA treatment, and right part of each panel present the ratio of treated group phenotypic data to the average of untreated group phenotypic data within the same genotype. Data are means ± SD. Each genotype contained eight randomly selected accessions, at least six seedlings were counted for each accession, and replicate three times. *NO* refers *Rht-B1aRht-D1a*, *B1b* refers *Rht-B1bRht-D1a*, *D1b* refers *Rht-B1aRht-D1b*. "*" indicates significant difference (Student's *t*-test $P < 0.01$) between with and without GA treatment. Different letters (a and b) on the top indicate significant differences ($P < 0.01$) between different genotypes with multiple comparisons in a treated group by least significant difference (LSD) test.

Figure S3. The above- and under-ground phenotypes of different genotype with and without exogenous BL treatment.

The indicated concentrations of BL were applied on the seedlings from 1 to 14 DAGs. Left part of each panel present the phenotypic data without BL treatment, and right part of each panel present the ratio of treated group phenotypic data to the average of untreated group phenotypic data within the same genotype. Data are means ± SD. Each genotype contained eight randomly selected accessions, at least six seedlings were counted for each accession, and replicate three times. *NO* refers *Rht-B1aRht-D1a*, *B1b* refers *Rht-B1bRht-D1a*, *D1b* refer *Rht-B1aRht-D1b*. "*" indicates significant difference (Student's *t*-test $P < 0.01$) between with and without BL treatment. Different letters (a and b) on the top indicate significant differences ($P < 0.01$) between different genotypes with multiple comparisons in a treated group by LSD test.

Supplemental Data

Table S1. Information of all accessions involved in this study.

Table S2. The validation of identified SNPs in population transcriptomic analysis.

Table S3. Gene ontology enrichment of the highly and lowly expressed genes.

Table S4. Gene ontology enrichment of the highly and lowly varied expression genes.

Table S5. The identified DEGs between LA and MC groups.

Table S6. Gene ontology enrichment of the DEGs between LA and MC.

Table S7. The DEGs related to root development between LA and MC.

Table S8. GWAS results of the root surface and volume at 14 DAGs.

Table S9. GWAS results of the adjusted root phenotypes at 14 DAGs.

Table S10. The accession list for phytohormones treatment.

Table S11. Genes co-expressed with *Rht-A1*, *Rht-B1* and *Rht-D1* genes.

Table S12. The identified DEGs between NO and D1b groups.

Table S13. The identified DEGs between NO and B1b groups.

Table S14. Gene ontology enrichment of the DEGs in D1b/NO and B1b/NO comparisons.

Table S15. GWAS results of the root-shoot ratio at 7 DAGs.

Table S16. The validation of identified SNP by the two biological replications RNA-seq.

Table S17. Imputation accuracy of SNPs under different cutoffs of missing rate.

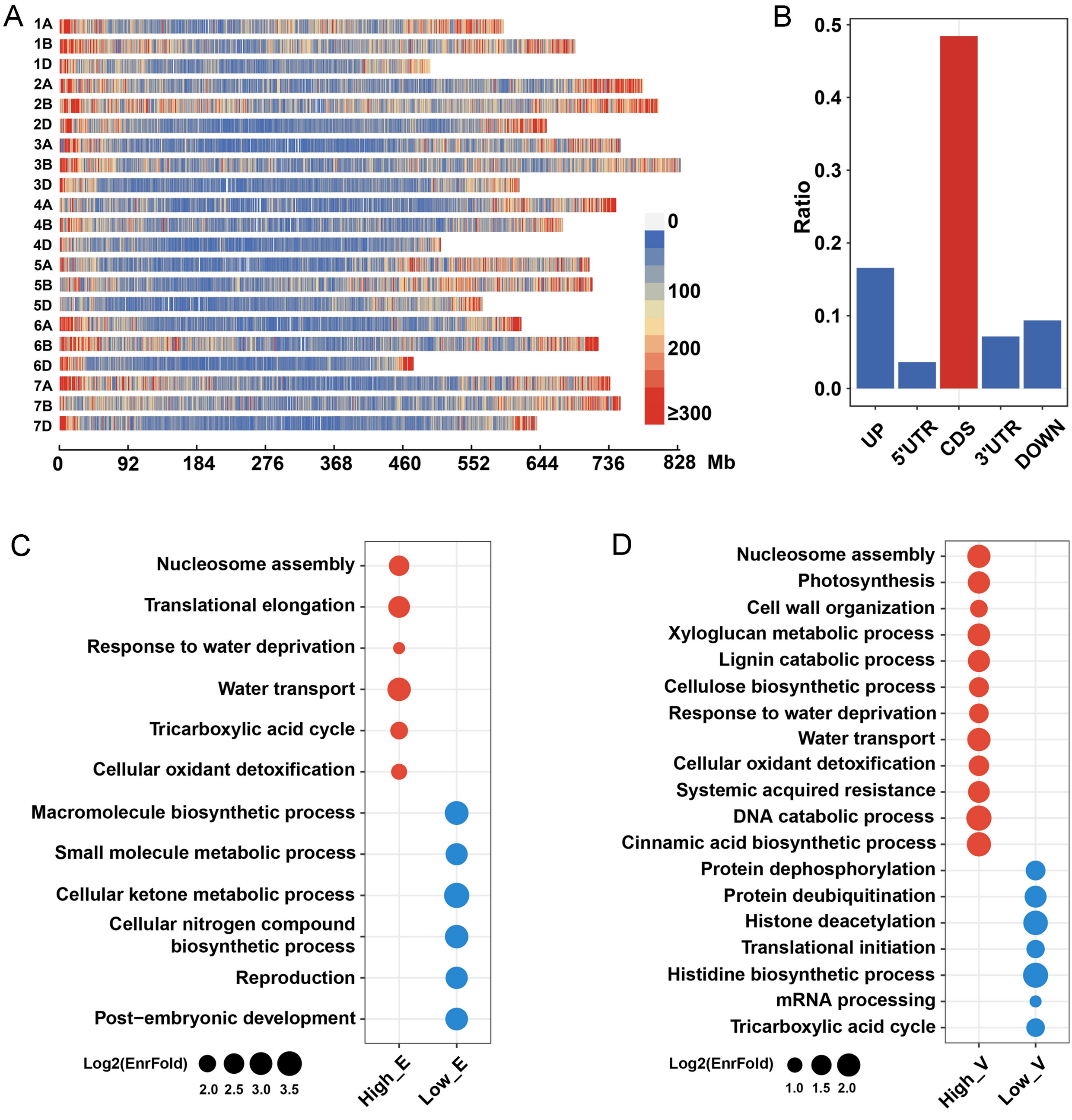
A
1A
1B
1D
2A
2B
2D
3A
3B
3D
4A
4B
4D
5A
5B
5D
6A
6B
6D
7A
7B
7D
0
100
200
≥300
0
92
184
276
368
460
552
644
736
828
Mb
B
Ratio
0.5
0.4
0.3
0.2
0.1
0.0
UP
5'UTR
CDS
3'UTR
DOWN
C
Nucleosome assembly
Translational elongation
Response to water deprivation
Water transport
Tricarboxylic acid cycle
Cellular oxidant detoxification
Macromolecule biosynthetic process
Small molecule metabolic process
Cellular ketone metabolic process
Cellular nitrogen compound biosynthetic process
Reproduction
Post−embryonic development
Log2(EnrFold)
2.0 2.5 3.0 3.5
High_E
Low_E
D
Nucleosome assembly
Photosynthesis
Cell wall organization
Xyloglucan metabolic process
Lignin catabolic process
Cellulose biosynthetic process
Response to water deprivation
Water transport
Cellular oxidant detoxification
Systemic acquired resistance
DNA catabolic process
Cinnamic acid biosynthetic process
Protein dephosphorylation
Protein deubiquitination
Histone deacetylation
Translational initiation
Histidine biosynthetic process
mRNA processing
Tricarboxylic acid cycle
Log2(EnrFold)
1.0 1.5 2.0
High_V
Low_V

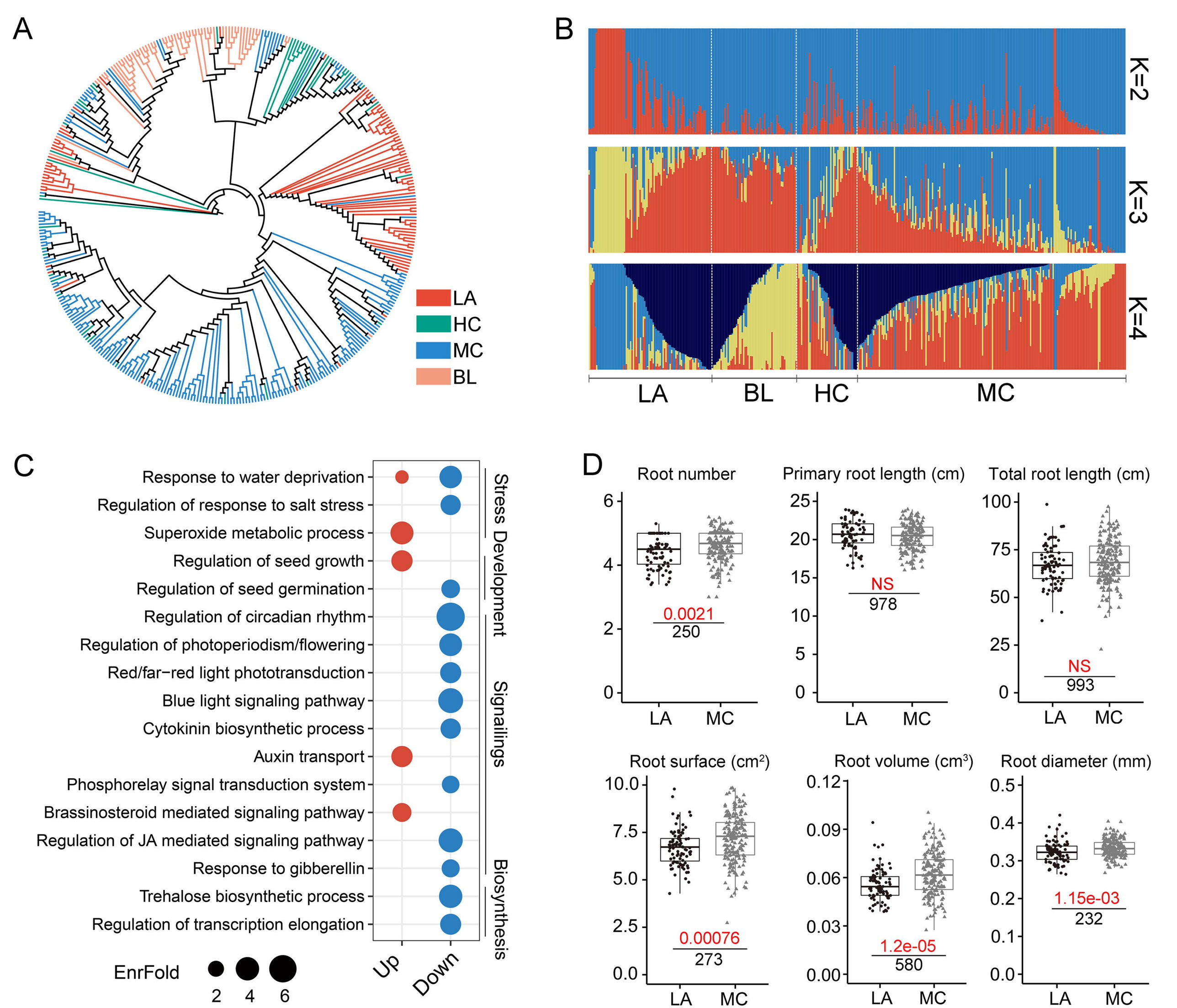
A
LA
HC
MC
BL
B
K=2
K=3
K=4
LA
BL
HC
MC
C
Response to water deprivation
Regulation of response to salt stress
Superoxide metabolic process
Regulation of seed growth
Regulation of seed germination
Regulation of circadian rhythm
Regulation of photoperiodism/flowering
Red/far−red light phototransduction
Blue light signaling pathway
Cytokinin biosynthetic process
Auxin transport
Phosphorelay signal transduction system
Brassinosteroid mediated signaling pathway
Regulation of JA mediated signaling pathway
Response to gibberellin
Trehalose biosynthetic process
Regulation of transcription elongation
Stress
Development
Signailings
Biosynthesis
Up
Down
EnrFold
2
4
6
D
Root number
0.0021
250
Primary root length (cm)
NS
978
Total root length (cm)
NS
993
Root surface (cm²)
0.00076
273
Root volume (cm³)
1.2e-05
580
Root diameter (mm)
1.15e-03
232
LA
MC

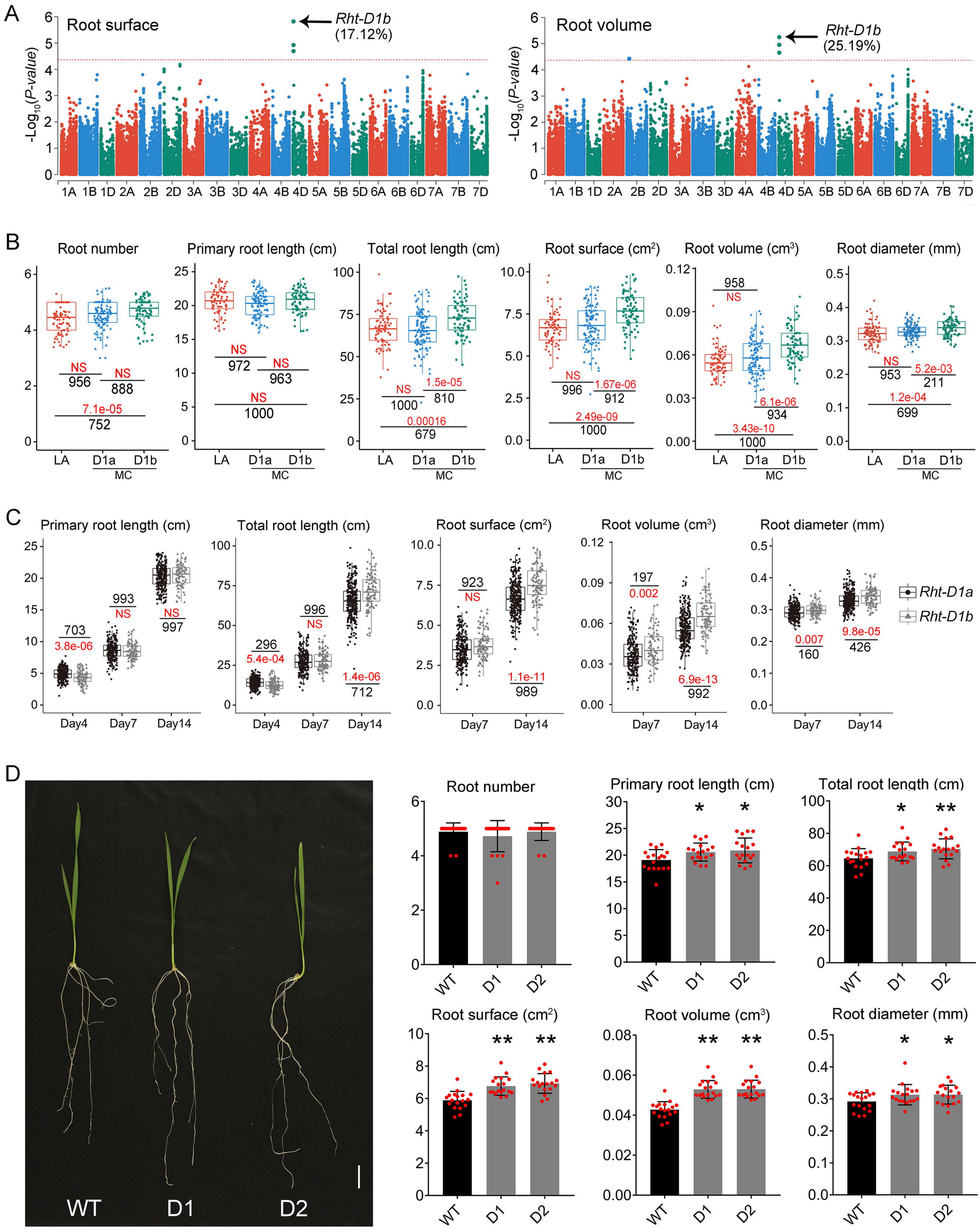
A
Root surface
Rht-D1b
(17.12%)
Root volume
Rht-D1b
(25.19%)
-Log10(P-value)
1A 1B 1D 2A 2B 2D 3A 3B 3D 4A 4B 4D 5A 5B 5D 6A 6B 6D 7A 7B 7D
B
Root number
Primary root length (cm)
Total root length (cm)
Root surface (cm2)
Root volume (cm3)
Root diameter (mm)
LA
D1a
D1b
MC
NS
956
888
7.1e-05
752
972
963
1000
1000
810
1.5e-05
0.00016
679
996
912
1.67e-06
2.49e-09
958
934
6.1e-06
3.43e-10
953
211
5.2e-03
1.2e-04
699
C
Primary root length (cm)
Total root length (cm)
Root surface (cm2)
Root volume (cm3)
Root diameter (mm)
Day4
Day7
Day14
703
3.8e-06
993
997
296
5.4e-04
996
712
1.4e-06
923
989
1.1e-11
197
0.002
992
6.9e-13
160
0.007
426
9.8e-05
Rht-D1a
Rht-D1b
D
WT
D1
D2
Root number
Primary root length (cm)
Total root length (cm)
Root surface (cm2)
Root volume (cm3)
Root diameter (mm)

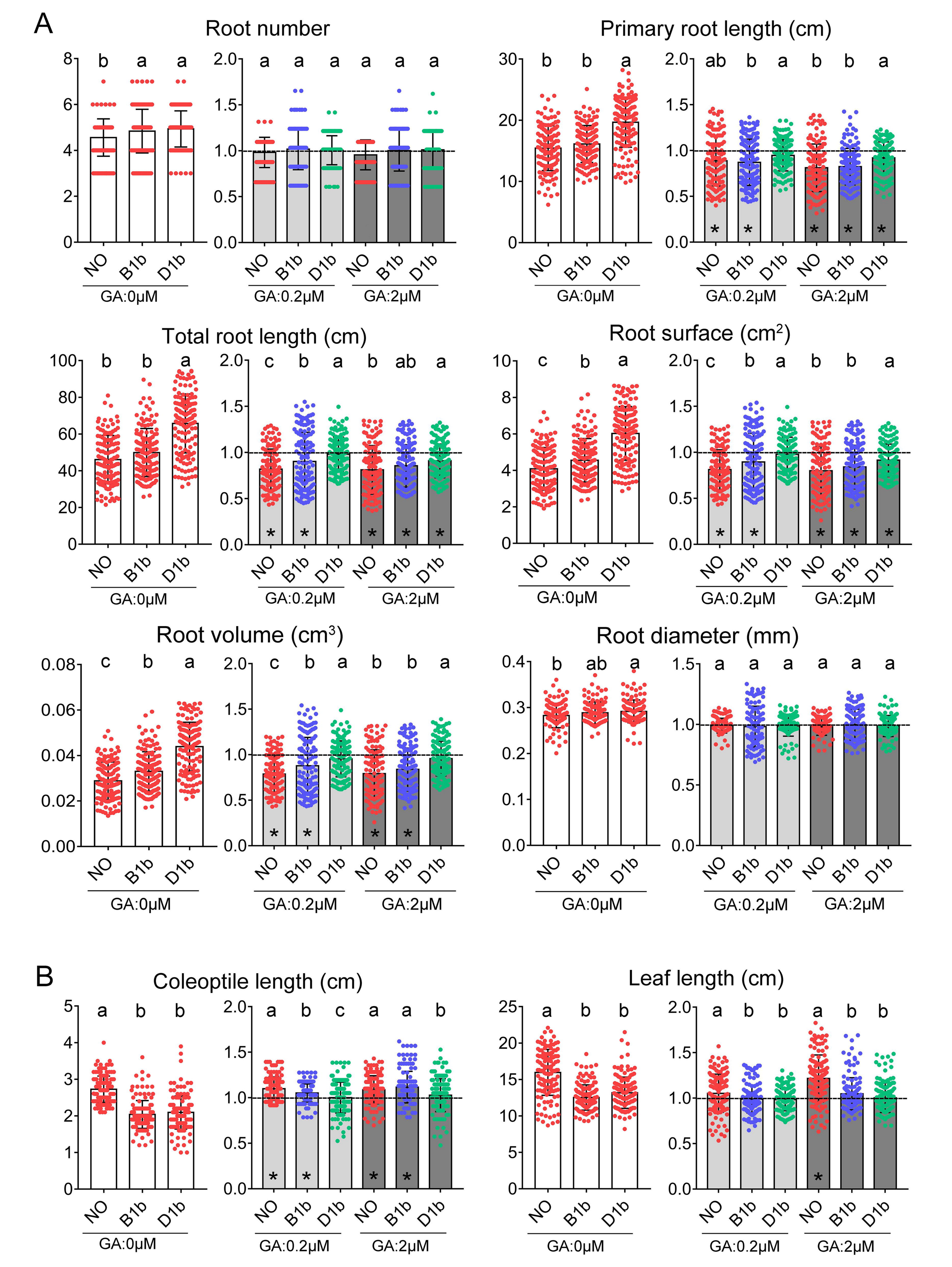
A
Root number
Primary root length (cm)
Total root length (cm)
Root surface (cm²)
Root volume (cm³)
Root diameter (mm)
B
Coleoptile length (cm)
Leaf length (cm)
NO
B1b
D1b
GA:0μM
GA:0.2μM
GA:2μM

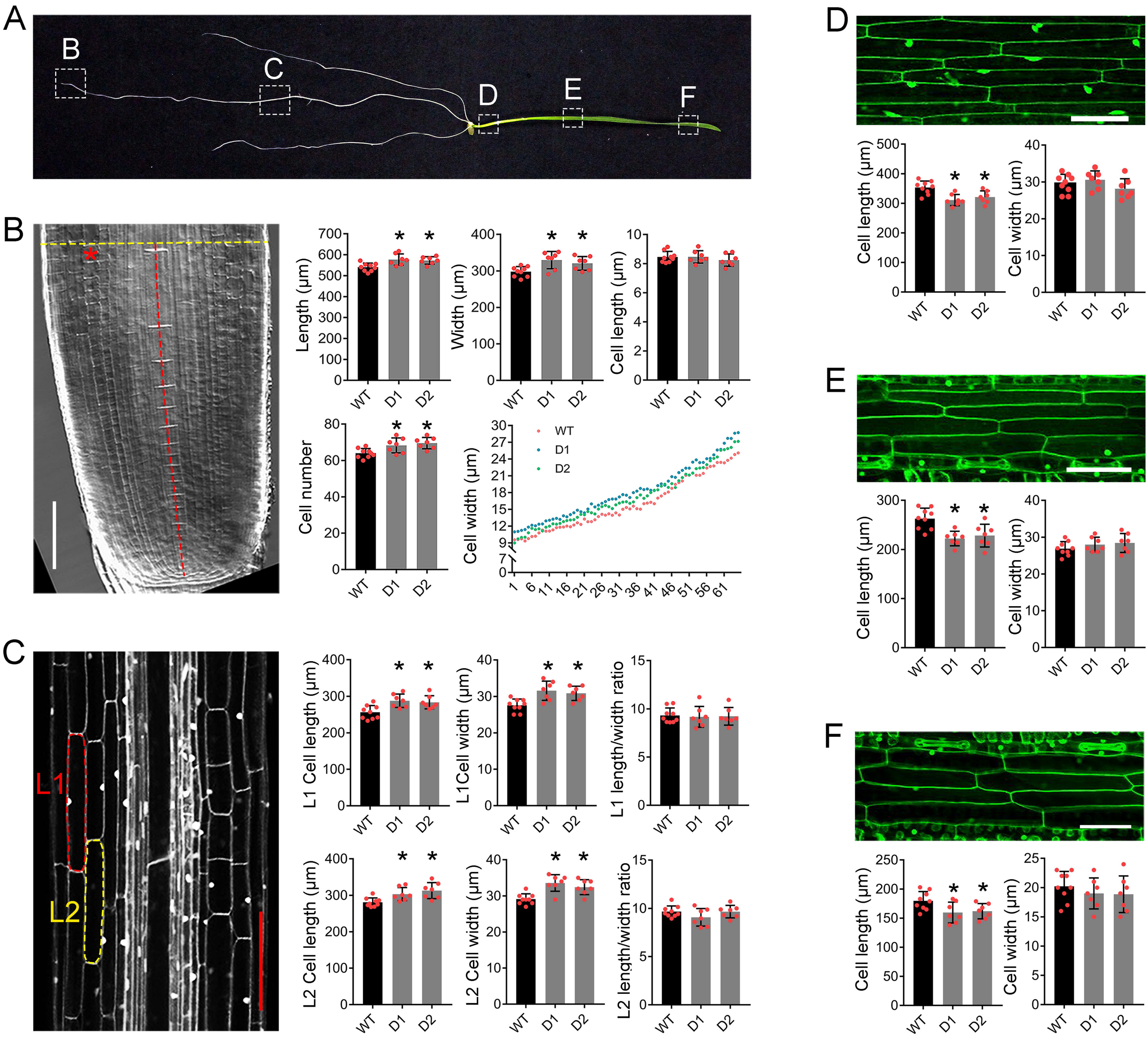
A
B
C
D
E
F
Length (μm)
Width (μm)
Cell length (μm)
Cell number
Cell width (μm)
WT
D1
D2
L1
L2
L1 Cell length (μm)
L1Cell width (μm)
L1 length/width ratio
L2 Cell length (μm)
L2 Cell width (μm)
L2 length/width ratio

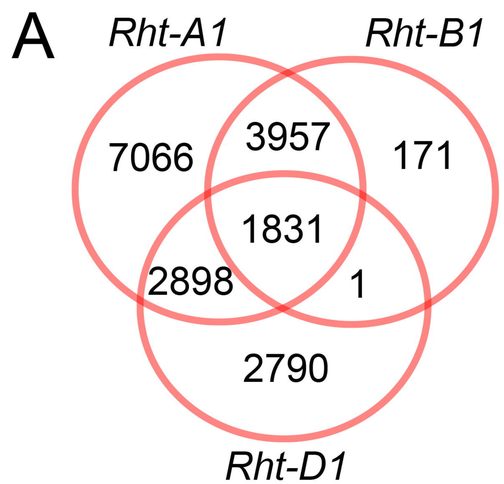
A
Rht-A1
Rht-B1
Rht-D1
7066
3957
171
1831
2898
1
2790

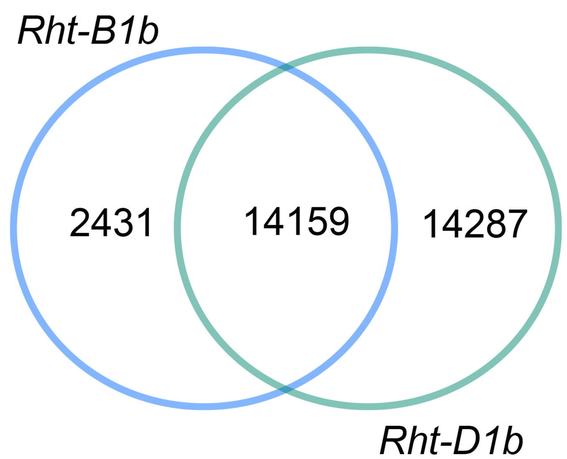
Rht-B1b
Rht-D1b
2431
14159
14287

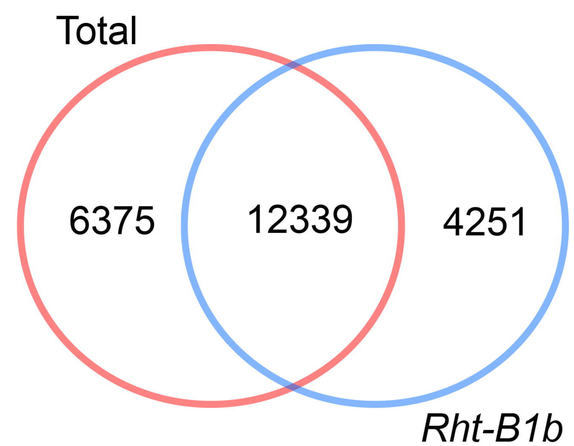
Total
Rht-B1b
6375
12339
4251

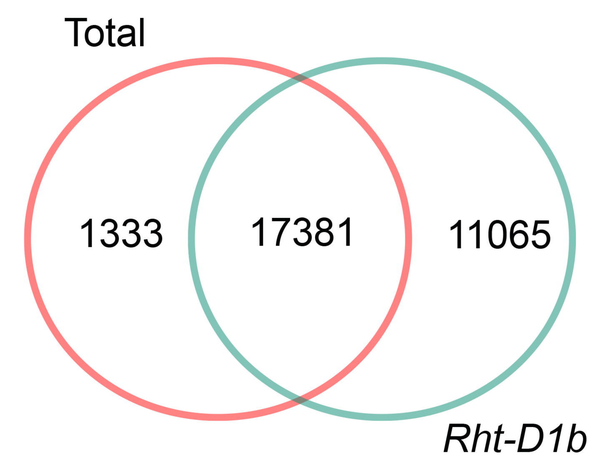
Total
Rht-D1b
1333
17381
11065

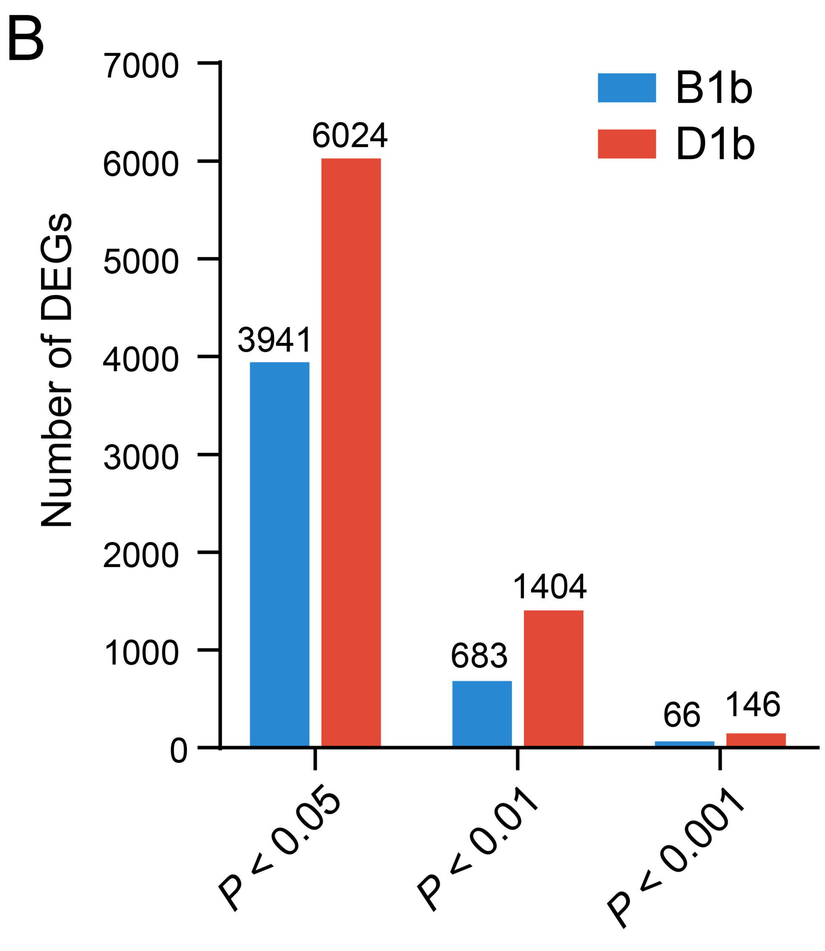
B
B1b
D1b
Number of DEGs
7000
6000
5000
4000
3000
2000
1000
0
3941
6024
683
1404
66
146
P < 0.05
P < 0.01
P < 0.001

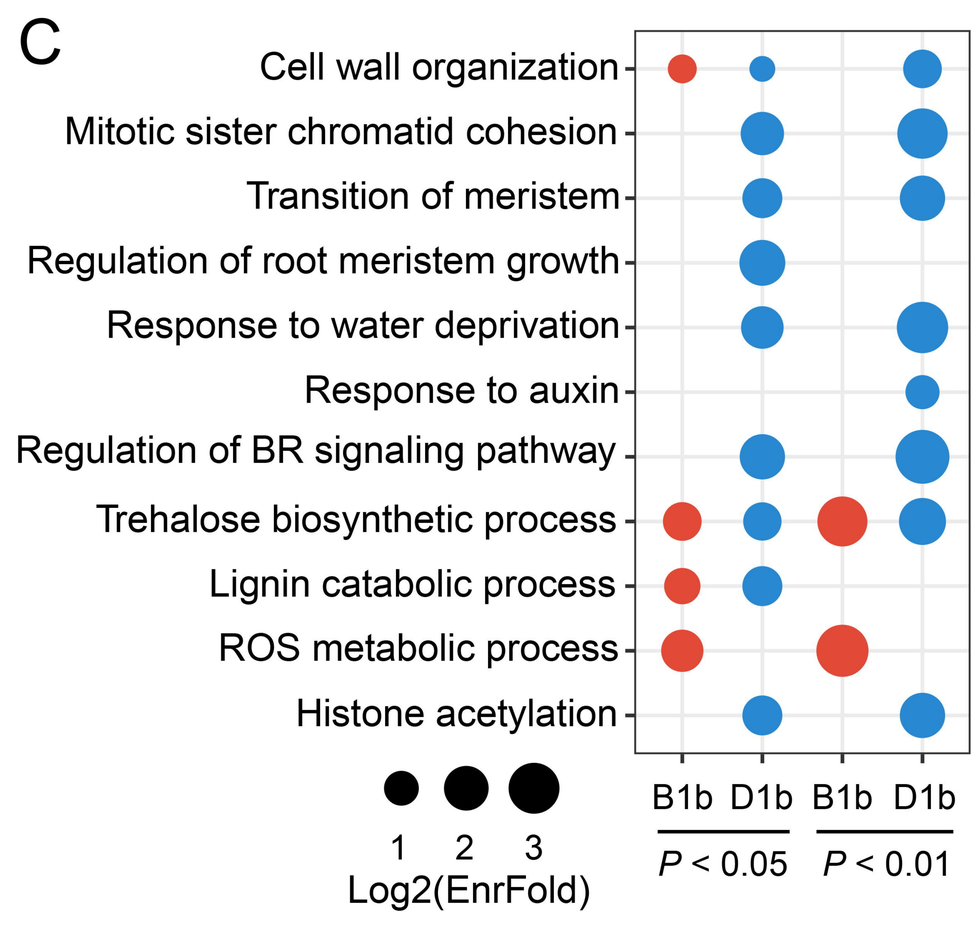
C
Cell wall organization
Mitotic sister chromatid cohesion
Transition of meristem
Regulation of root meristem growth
Response to water deprivation
Response to auxin
Regulation of BR signaling pathway
Trehalose biosynthetic process
Lignin catabolic process
ROS metabolic process
Histone acetylation
1
2
3
Log2(EnrFold)
B1b
D1b
B1b
D1b
P < 0.05
P < 0.01

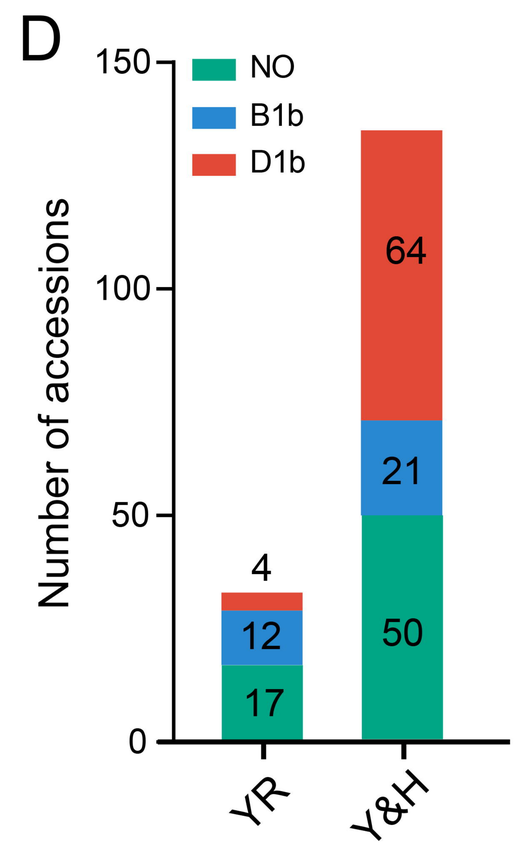
D
NO
B1b
D1b
Number of accessions
150
100
50
0
4
12
17
64
21
50
YR
Y&H

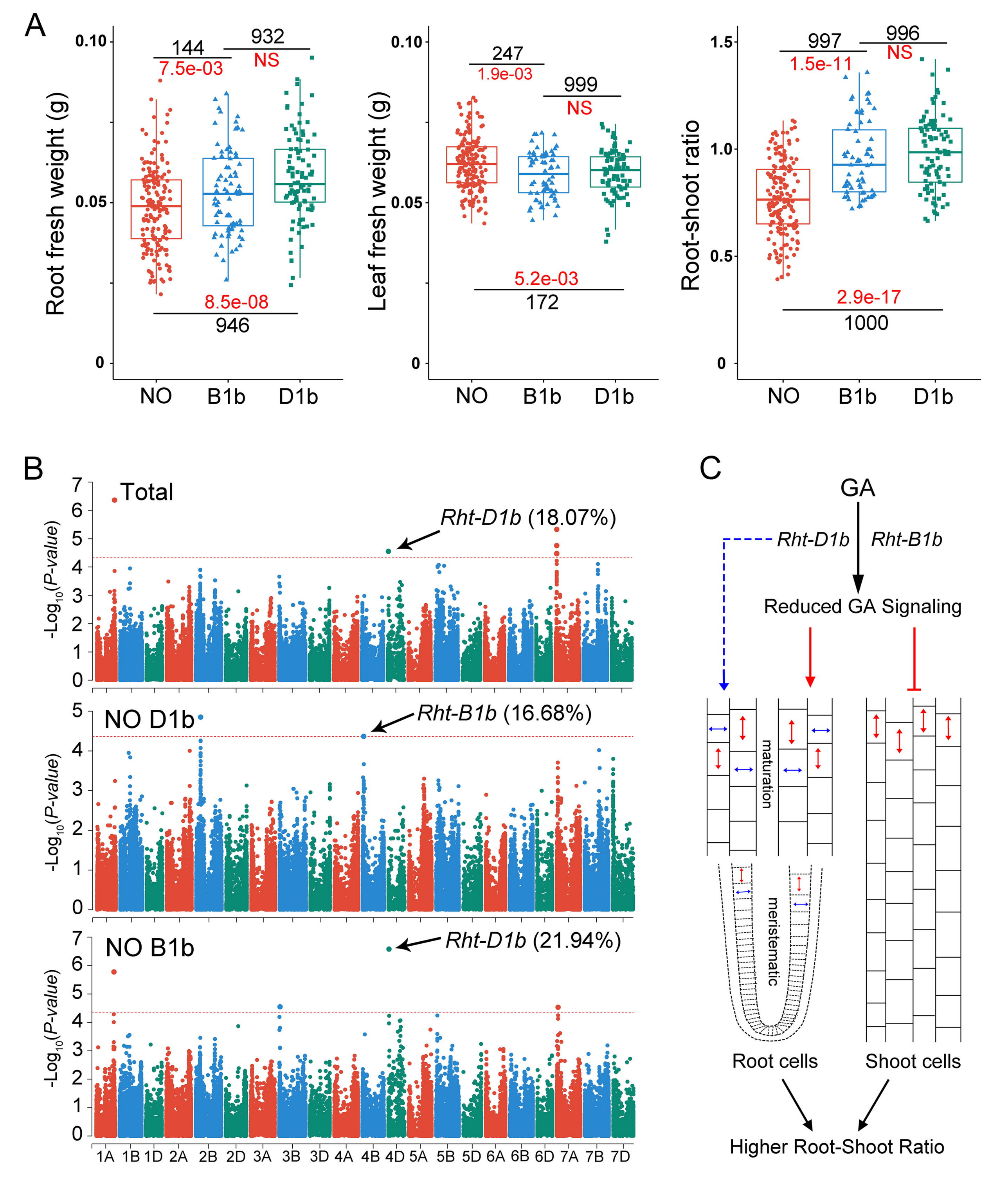
A
Root fresh weight (g)
144
7.5e-03
932
NS
8.5e-08
946
NO
B1b
D1b
Leaf fresh weight (g)
247
1.9e-03
999
NS
5.2e-03
172
Root-shoot ratio
997
1.5e-11
996
NS
2.9e-17
1000
B
Total
Rht-D1b (18.07%)
NO D1b
Rht-B1b (16.68%)
NO B1b
Rht-D1b (21.94%)
-Log10(P-value)
1A 1B 1D 2A 2B 2D 3A 3B 3D 4A 4B 4D 5A 5B 5D 6A 6B 6D 7A 7B 7D
C
GA
Rht-D1b
Rht-B1b
Reduced GA Signaling
maturation
meristematic
Root cells
Shoot cells
Higher Root-Shoot Ratio

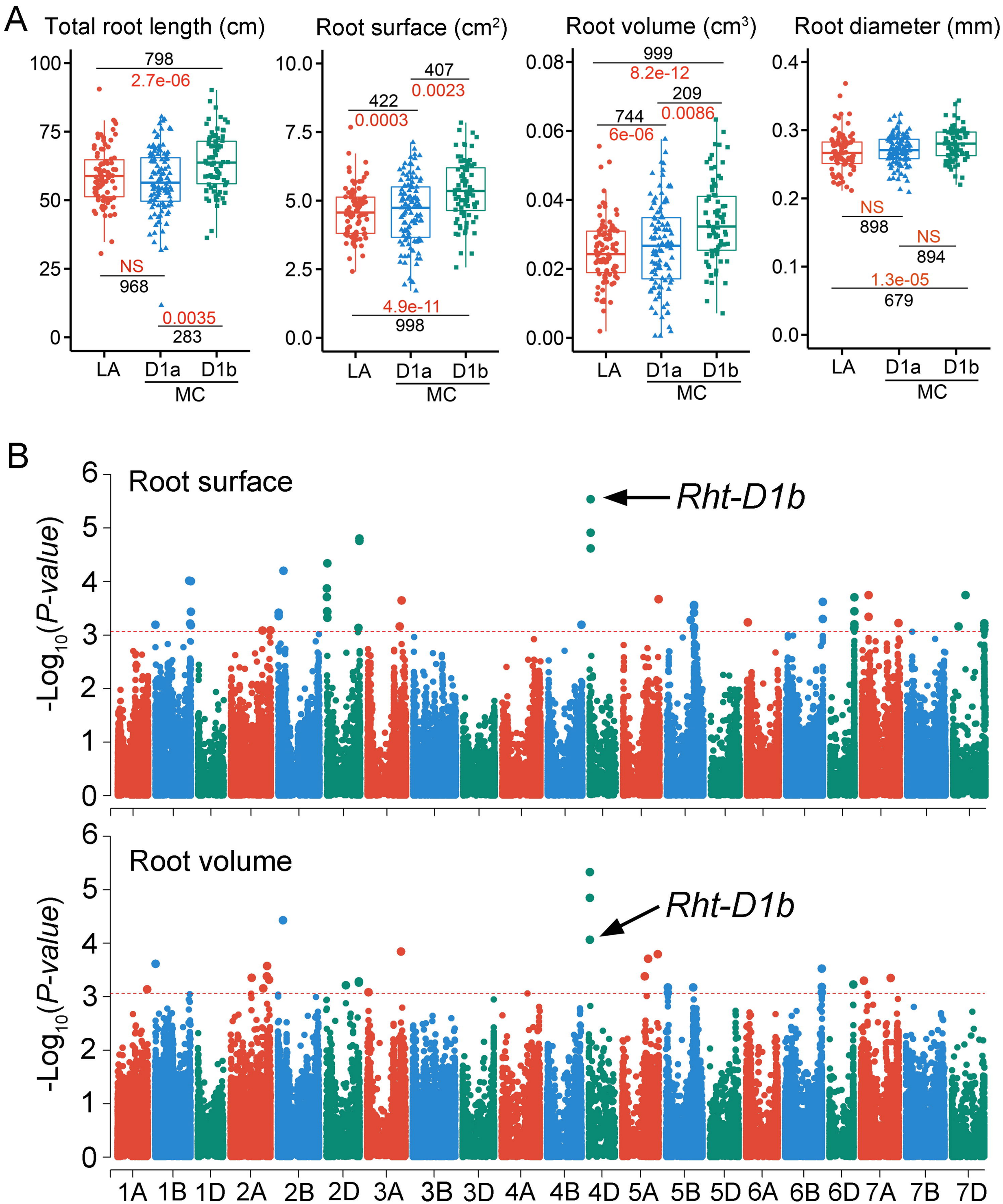
A
Total root length (cm)
Root surface (cm²)
Root volume (cm³)
Root diameter (mm)
798
2.7e-06
NS
968
0.0035
283
407
0.0023
422
0.0003
4.9e-11
998
999
8.2e-12
209
0.0086
744
6e-06
NS
898
NS
894
1.3e-05
679
LA
D1a
D1b
MC
B
Root surface
Rht-D1b
Root volume
Rht-D1b
-Log10(P-value)
1A 1B 1D 2A 2B 2D 3A 3B 3D 4A 4B 4D 5A 5B 5D 6A 6B 6D 7A 7B 7D

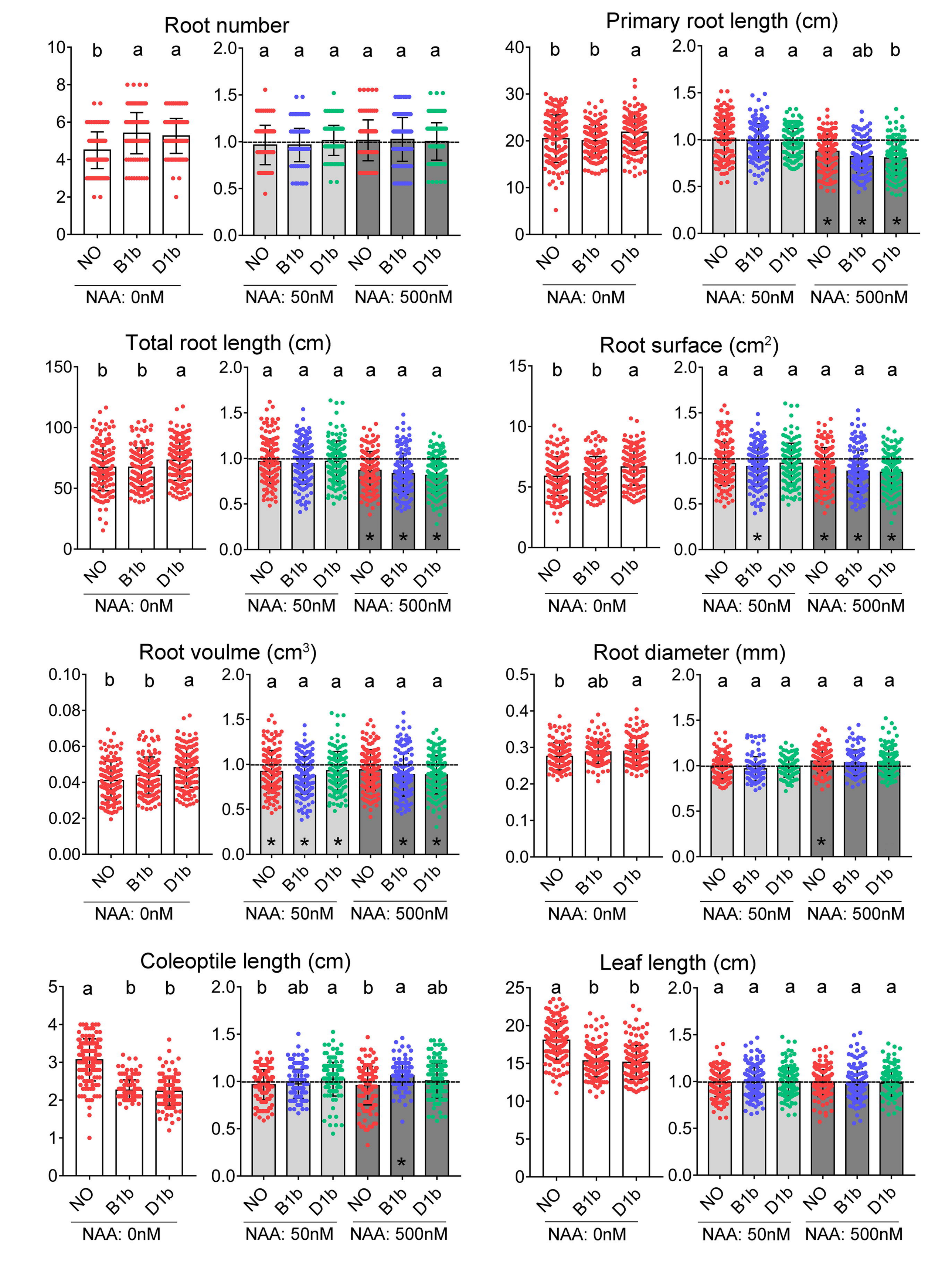
Root number
Primary root length (cm)
Total root length (cm)
Root surface (cm²)
Root voulme (cm³)
Root diameter (mm)
Coleoptile length (cm)
Leaf length (cm)
NO
B1b
D1b
NAA: 0nM
NAA: 50nM
NAA: 500nM

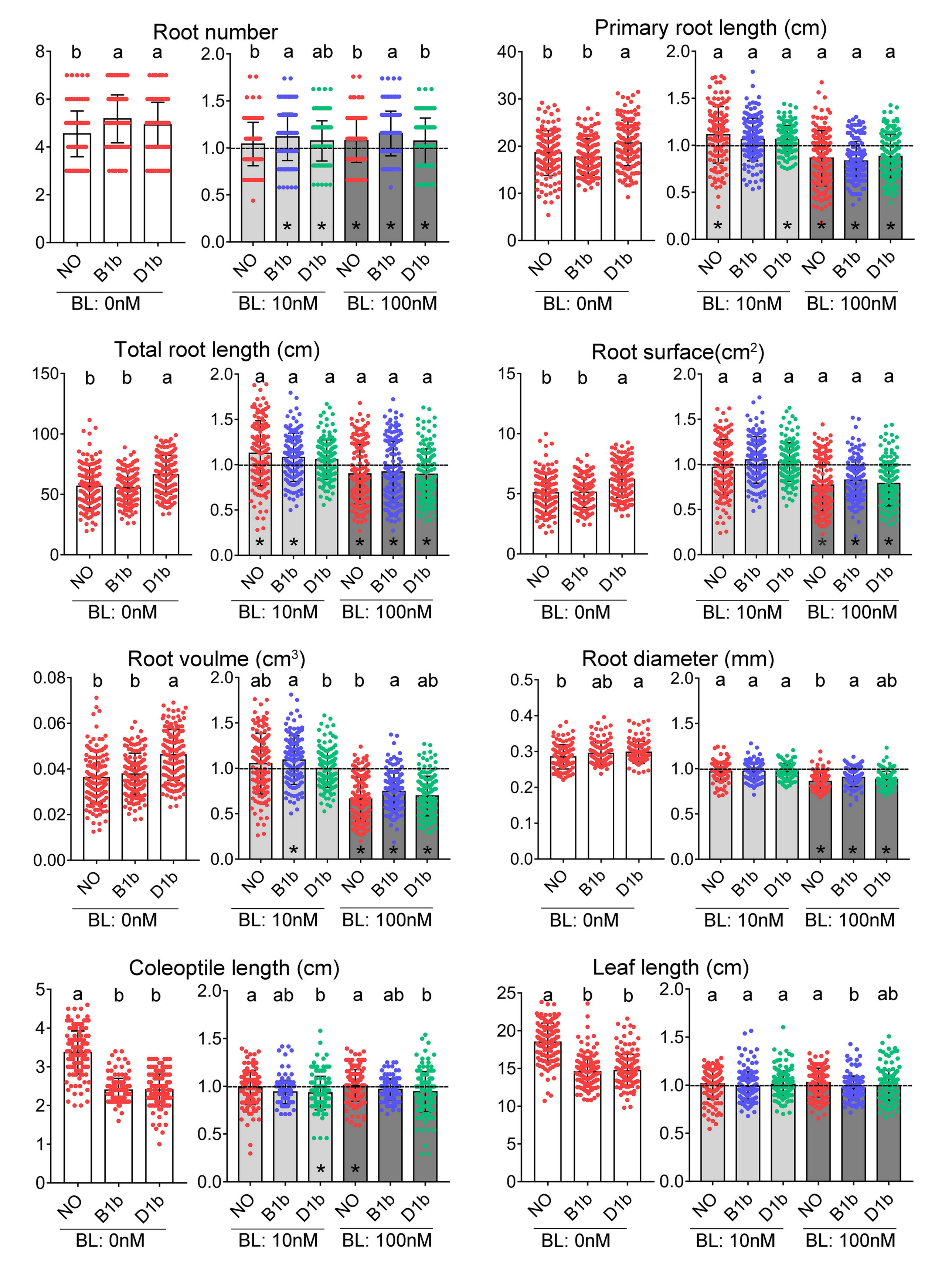
Root number
Primary root length (cm)
Total root length (cm)
Root surface(cm²)
Root voulme (cm³)
Root diameter (mm)
Coleoptile length (cm)
Leaf length (cm)
NO
B1b
D1b
BL: 0nM
BL: 10nM
BL: 100nM